NATIONAL ADVISORY COMMITTEE FOR AERONAUTICS

TECHNICAL NOTE 2358

EFFECT OF VERTICAL-TAIL AREA AND LENGTH ON THE YAWING STABILITY CHARACTERISTICS OF A MODEL HAVING A 45° SWEPTBACK WING

By William Letko

Langley Aeronautical Laboratory
Langley Field, Va.

Washington
May 1951

NATIONAL ADVISORY COMMITTEE FOR AERONAUTICS

TECHNICAL NOTE 2358

EFFECT OF VERTICAL-TAIL AREA AND LENGTH ON THE YAWING STABILITY CHARACTERISTICS OF A MODEL HAVING A 45° SWEPTBACK WING

By William Letko

SUMMARY

An investigation was made to evaluate the contributions to yawing stability derivatives of the various airplane components and to determine the interference between the components of a high-speed-airplane configuration having different tail areas and tail lengths. The model was equipped with a 45° sweptback wing of aspect ratio 4. The results indicate that, for the midwing arrangements investigated, the effects of wing-fuselage interference were small over the greater part of the angle-of-attack range. Although rather large interference effects on vertical-tail effectiveness appeared to be produced by the fuselage and by the wing at moderate and high angles of attack, these interference effects tended to cancel each other and, therefore, had little influence on tail effectiveness for the complete configurations. The fuselage had little influence on the effective aspect ratio of the vertical tail at 0° angle of attack in the yawing condition. Addition of the horizontal tail produced an increase in effective aspect ratio equivalent to that obtained in static-stability tests for a fuselage - horizontal-tail combination. For the configurations tested, the tail contributions to the yawing derivatives were estimated fairly accurately for most of the angle-of-attack range by available procedures. The estimates based on the value of tail lift-curve slope at 0° angle of attack of the model gave, for the medium and long tail lengths, somewhat better results up to the angle of attack of maximum lift than calculations based on values of the lateral force due to yaw angle measured through the angle-of-attack range. Addition of a full-span slat to the wing had only a slight effect on the effectiveness of the vertical tail at 0° angle of attack.

INTRODUCTION

The necessity for design changes of main components of airplanes to meet the demands of high-speed flight has led to consideration of some unusual configurations. For many of these components, complete design

information regarding stability characteristics is unavailable. The effects of changes in wing design on stability characteristics have been extensively investigated. In order to provide information on the influence of other parts of the complete airplane on the stability characteristics, an investigation of a model having various interchangeable components is being conducted in the Langley stability tunnel. References 1 and 2 present, respectively, the results of investigations to determine the effect of tail area and tail length and the effect of location of a swept horizontal tail on static lateral stability characteristics.

The present investigation was made to determine the effect of vertical-tail area and tail length on the low-speed yawing derivatives of a high-speed-airplane configuration. The investigation was also made to provide data for checking the validity of available procedures for estimating these tail effects on the yawing derivatives. In addition, the contributions to the yawing derivatives of the other components of the configuration were determined and the interference between the components of the configuration is shown.

SYMBOLS

The data are presented in the form of standard NACA coefficients of forces and moments which are referred to the stability axes with the origin at the projection on the plane of symmetry of the quarter-chord point of the wing mean aerodynamic chord and at the midpoint of the fuselage. The positive directions of the forces, moments, and angular displacements are shown in figure 1. The coefficients and symbols are defined as follows:

A	aspect ratio (b^2/S)
b	wing span, measured perpendicular to axis of symmetry, feet
c	chord, measured parallel to plane of symmetry, feet
$\bar{c}$	mean aerodynamic chord, feet $\left(\frac{2}{S}\int_0^{b/2} c^2 dy\right)$
d	fuselage ordinate measured normal to fuselage axis (see table I)
l	fuselage length, feet
l_V	distance from origin of axis $l/2$ to $\bar{c}/4$ of vertical and horizontal tail, feet

q	dynamic pressure, pounds per square foot $\left(\frac{1}{2}\rho V^2\right)$
r	yawing angular velocity, radians per second
$rb/2V$	yawing-velocity parameter
s	distance along fuselage axis, measured rearward from fuselage nose
S	area, square feet
V	velocity, feet per second
y	spanwise distance measured from plane of symmetry, feet
z_V	perpendicular distance from fuselage center line to quarter chord of mean aerodynamic chord of vertical tail, feet
α	angle of attack of model, degrees
Λ	angle of sweepback of quarter-chord line, degrees
ρ	mass density, slugs per cubic foot
ψ	angle of yaw, degrees
Z	normal force
L	lift; $L = -Z$ force in figure 1
D	drag
X	longitudinal force; $X = -D$ at $\psi = 0^\circ$
Y	lateral force
L'	rolling moment
M	pitching moment
N	yawing moment
C_D	drag coefficient (D/qS_W); $C_D = -C_X$ at $\psi = 0^\circ$
C_L	lift coefficient (L/qS_W)

C_X longitudinal-force coefficient (X/qS_W)

C_Y lateral-force coefficient (Y/qS_W)

C_l rolling-moment coefficient (L'/qS_Wb)

C_m pitching-moment coefficient $(M/qS_W\bar{c}_W)$

C_n yawing-moment coefficient (N/qS_Wb)

$$C_{Y_\psi} = \frac{\partial C_Y}{\partial \psi}$$

$$C_{l_r} = \frac{\partial C_l}{\partial \frac{rb}{2V}}$$

$$C_{Y_r} = \frac{\partial C_Y}{\partial \frac{rb}{2V}}$$

$$C_{n_r} = \frac{\partial C_n}{\partial \frac{rb}{2V}}$$

$\left(C_{L_\alpha}\right)_V$ lift-curve slope of vertical tail (C_L of vertical tail based on vertical-tail area)

$\Delta_1 C_{Y_r}$, $\Delta_1 C_{n_r}$, $\Delta_1 C_{l_r}$ increments of coefficients caused by wing-fuselage interference; that is,

$$\Delta_1 C_{Y_r} = \left(C_{Y_r}\right)_{W+F} - \left(C_{Y_r}\right)_W - \left(C_{Y_r}\right)_F$$

$\Delta_2 C_{n_r}$ increment of coefficients caused by wing-fuselage interference on vertical-tail effectiveness or on complete-tail effectiveness; that is, for horizontal tail off,

$$\Delta_2 C_{n_r} = \left[\left(C_{n_r}\right)_{W+F+V} - \left(C_{n_r}\right)_{W+F}\right] - \left[\left(C_{n_r}\right)_{F+V} - \left(C_{n_r}\right)_{F}\right]$$

and, for horizontal tail on,

$$\Delta_2 C_{n_r} = \left[\left(C_{n_r}\right)_{W+F+H+V} - \left(C_{n_r}\right)_{W+F}\right] - \left[\left(C_{n_r}\right)_{F+H+V} - \left(C_{n_r}\right)_{F}\right]$$

$\Delta_3 C_{n_r}$ increment of coefficients caused by fuselage interference on vertical-tail effectiveness or on complete-tail effectiveness; that is, for horizontal tail off,

$$\Delta_3 C_{n_r} = \left[\left(C_{n_r}\right)_{F+V} - \left(C_{n_r}\right)_{F}\right] - \left[\left(C_{n_r}\right)'_{V}\right]$$

and, for horizontal tail on,

$$\Delta_3 C_{n_r} = \left[\left(C_{n_r}\right)_{F+H+V} - \left(C_{n_r}\right)_{F}\right] - \left[\left(C_{n_r}\right)'_{H+V}\right]$$

where prime indicates contribution of isolated tail

Subscripts and abbreviations:

e	effective
F	fuselage; used with subscripts 1 to 3 to denote the various fuselages (see fig. 3)
H	horizontal tail
S	slat
V	vertical tail; used with subscripts 1 to 3 to denote various vertical tails (see fig. 2)
W	wing

APPARATUS AND MODELS

The tests were made in the 6- by 6-foot curved-flow test section of the Langley stability tunnel. In this test section, curved flight is simulated by causing air to flow in a curved path about a fixed model.

The general research models used for the present investigation were designed to permit tests of the wing alone, fuselage alone, or the fuselage in combination with any of several tail configurations with or without the wing.

Three circular-arc fuselages of circular cross section were used in the investigation to obtain a variation in tail length. The fuselages had the same maximum diameter and were of fineness ratios of 5.00, 6.67, and 10.00 with ratios of tail length to wing span of 0.347, 0.464, and 0.697, respectively. The coordinates of the fuselages are given in table I. The sizes of the tails were selected to give ratios of tail area to wing area of 0.075, 0.150, and 0.225.

For some of the tests, the wing was equipped with a full-span slat. The slat chord was 8 percent of the wing chord. Details of the wing, slat, fuselages, and tail surfaces and the relative locations of these components are given in figures 2 to 4. The various fuselages and vertical tails henceforth are referred to by the number and symbol assigned to them in figures 2 and 3. A photograph of one of the test configurations is given as figure 5. The pertinent geometric characteristics are given in table II.

For the tests, the model was mounted on a single-strut support at the quarter-chord point of the wing mean aerodynamic chord, which coincided with the 50-percent point of the fuselage length. Forces and moments were measured by means of a conventional six-component balance system.

TESTS

All the tests were made at a dynamic pressure of 24.9 pounds per square foot, which corresponds to a Mach number of 0.13. The test Reynolds number, based on the mean aerodynamic chord of the wing, was about 0.71×10^6.

The angle-of-attack range for both the tests in straight flow and in yawing flow was from about -6° up to about 32°. In straight flow, the lift, longitudinal force, and pitching moments were determined. The yawing derivatives were determined by measuring the side force, yawing moment, and rolling moment at values of $rb/2V$ of 0, -0.0316, -0.0670, and -0.0883. The test configurations are presented in table III.

CORRECTIONS

Approximate corrections, based on unswept-wing theory, for the effects of jet boundaries have been applied to the angle of attack, the pitching-moment coefficient, the longitudinal-force coefficient, and the rolling-moment coefficient. The lateral-force coefficients have been corrected for the buoyancy effect of the static-pressure gradient associated with curved flow.

Corrections for the effects of blocking, turbulence, or static-pressure gradient on the boundary-layer flow have not been applied to the data.

RESULTS AND DISCUSSION

Presentation of Results

The results of the present investigation are presented essentially in two parts. The first part, consisting of figures 6 to 16, presents data as obtained from tests. The second part consists of figures 17 to 26 made to facilitate the analysis.

The test configurations for which data are presented in figures 6 to 16 are summarized in table III.

Contributions of Wing-Fuselage Combination to Yawing Stability Derivatives

General discussion.- In order to determine the contribution of the wing-fuselage combination to the stability derivatives, the separate contributions of the wing and fuselage must either be known from tests or must be estimated. Also, the sum of the separate contributions must be corrected for mutual interference effects of the wing and fuselage if this interference appears to be significant. In accordance with conventional procedures (reference 3), the contribution of the wing-fuselage combination to C_{n_r}, for example, can be written as

$$\left(C_{n_r}\right)_{W+F} = \left(C_{n_r}\right)_W + \left(C_{n_r}\right)_F + \Delta_1 C_{n_r} \qquad (1)$$

where $(C_{n_r})_W$ and $(C_{n_r})_F$ are the separate contributions of the wing and fuselage, respectively, and $\Delta_1 C_{n_r}$ is the increment caused by mutual interference of the wing and fuselage. The wing and fuselage contributions and the interference increments obtained will be discussed separately in the following sections.

Wing characteristics.- The lift, drag, and pitching-moment characteristics of the wing alone, with and without a leading-edge slat are presented in figure 6. The characteristics of the wing alone were discussed in reference 2 and since the data of reference 2 differ only slightly from the data obtained in the present tests no discussion of these characteristics is presented herein. The data are presented only to facilitate the analysis of the yawing stability derivatives. The data of figure 6 were obtained with a uniform turbulence screen about 10 feet ahead of the model. The screen was used to make the turbulence condition more nearly the same as that obtained in yawing flow. Screens of nonuniform wire spacing are used in yawing flow to obtain proper airstream curvature. Because of the different turbulence conditions, some small differences in the wing-alone data of reference 2 and figure 6 are to be expected. Previous tests with and without the uniform screen showed that turbulence effects on the static lateral stability derivatives of a wing were negligible.

In figure 17 is presented the variation of $C_D - \frac{C_L^2}{\pi A}$ with angle of attack for the wing alone and the wing with slat. It was pointed out in reference 4 that the quantity $C_D - \frac{C_L^2}{\pi A}$ begins to increase rapidly at the angle of attack at which flow separation begins. Abrupt changes in stability derivatives usually occur at about these same angles of attack. This tendency is particularly evident for the derivative C_{l_r}, shown in figure 7, for the wing with and without the slat, although the abrupt changes in C_{l_r} appear to occur at slightly smaller angles of attack than the abrupt changes in $C_D - \frac{C_L^2}{\pi A}$. Investigations involving Reynolds number as a variable have shown that for smooth wings, increases in Reynolds number tended to increase the angle of attack at which the initial changes occurred in plots of aerodynamic parameters against angle of attack and increased the angle of attack at which an abrupt change occurred in the increment $C_D - \frac{C_L^2}{\pi A}$. Effects of Reynolds number on the quantity $C_D - \frac{C_L^2}{\pi A}$, therefore, can be expected to provide an indication of effects of Reynolds number on the rotary stability derivatives. The values of C_{Y_r} and C_{n_r} for the plain wing and for the wing with slat are also shown in figure 7, and it can be seen that the values are small and differ appreciably only at angles of attack near maximum lift.

The values of C_{Y_r}, C_{n_r}, and C_{l_r} from figure 7 are plotted against lift coefficient in figure 8 and are compared with values computed by methods of reference 5. The calculated variation of C_{l_r} with lift coefficient agrees reasonably well with the results obtained for both the plain wing and for the wing with slat up to the lift coefficient which corresponds to the abrupt change in the increment $C_D - \frac{C_L^2}{\pi A}$ for each wing. The equation of reference 5 (equation (41)) for calculating C_{n_r} shows a dependence of C_{n_r} on the drag of the wing; therefore, two calculated results, which differ appreciably at the higher angles of attack where the drag of the wing alone and the wing with slat differ appreciably, are shown. The calculated results indicate more damping than the test results at all angles of attack below maximum lift, although the differences are rather small in the low angle-of-attack range. The calculated values of C_{Y_r} agree very well with the values measured for most of the lift-coefficient range. The calculated values agree with those measured for the wing with slat for a slightly larger range of lift coefficient than for those measured for the wing alone.

Fuselage and wing-fuselage characteristics.- The yawing derivatives of the fuselage of 6.67 fineness ratio (fuselage 2) are shown in figure 9. An interesting result shown is the change in sign of the rotary derivative C_{n_r} from negative values (positive damping) to positive values (negative damping) as the angle of attack is increased beyond 12°. A positive explanation of this characteristic is not known; however, it seems likely that, in a curved-flight path, a destabilizing sidewash at the rear part of the fuselage results from the disturbance created by the forward part of the fuselage when the angle of attack is high. For an oscillatory motion of the model some lag of sidewash might be expected and, therefore, it is probable that the effective damping derivative for an oscillatory motion of an isolated fuselage is considerably different from the steady curved-flight derivative shown in figure 9. Results obtained for three wing-fuselage combinations (figs. 10 to 12) showed no positive values of C_{n_r} below the angle of attack for maximum lift. This result is due in part to the damping contribution of the wing, but it is also probable that the adverse sidewash, referred to previously, is prevented by wing interference.

Wing-fuselage interference.- Rearranging the terms of equation (1) results in

$$\Delta_1 C_{n_r} = \left(C_{n_r}\right)_{W+F} - \left[\left(C_{n_r}\right)_W + \left(C_{n_r}\right)_F\right]$$

The interference increments $\Delta_1 C_{Y_r}$, $\Delta_1 C_{n_r}$, and $\Delta_1 C_{l_r}$ were determined in this manner from the test data for the wing in combination with fuselage 2. The increments are presented in figure 18 plotted against angle of attack. The increments are small over most of the angle-of-attack range. For configurations other than the midwing configuration tested, however, the increments would probably be larger even at small angles of attack.

Contributions of Tail to Yawing Stability Derivatives

The method of interference increments, which as mentioned before is analagous to methods used in previous work on static lateral stability, has been considered in the analysis of the tail contributions to the yawing stability derivatives. This method would indicate, for example, that

$$\left(C_{n_r}\right)_V = \left(C_{n_r}\right)_V' + \Delta_2 C_{n_r} + \Delta_3 C_{n_r}$$

where $\left(C_{n_r}\right)_V$ is the tail contribution with or without the horizontal tail. The prime indicates the contribution for the isolated tail. The increment $\Delta_2 C_{n_r}$ is the change in the tail contribution to C_{n_r} caused by wing interference effects, and $\Delta_3 C_{n_r}$ is the change in the tail contribution to C_{n_r} caused by fuselage interference effects. The increment $\Delta_3 C_{n_r}$ cannot be determined readily from measured results because it would necessitate acquiring measured values of $\left(C_{n_r}\right)_V'$. The fact that $\Delta_3 C_{n_r}$ is significant can be shown from figure 19 which presents values of $\left(C_{n_r}\right)_V$ determined from the basic data of figures 9 and 11. Figure 19 shows, for the wing-off condition, a large increase in the damping contribution of the tail with an increase in angle of attack. This increase is probably caused by fuselage sidewash effects on the vertical tail, because calculations of the tail contribution show little change with angle of attack. The curves of $\left(C_{n_r}\right)_V$ with the wing on also show very little variation with angle of attack. The wing interference on the tail contribution, therefore, must approximately cancel the fuselage interference for this configuration; that is,

$$\Delta_2 C_{n_r} + \Delta_3 C_{n_r} \approx 0$$

If fuselage sidewash is responsible for the increase of tail effectiveness with angle of attack when the wing is removed, then it might be expected that time-dependent effects will be involved in unsteady flight. As had been pointed out previously in connection with the discussion of the damping in yaw of the fuselage, the effective damping derivative for an oscillatory motion of the model might therefore be expected to be different from the damping derivative for steady-turning flight because of lag of sidewash. Apparently, the effect of the wing largely cancels the sidewash effects of the fuselage so that the tail contributions to the yawing derivatives with wing on should be unaffected by these sidewash effects for either steady-turning or oscillatory motions. This statement cannot be expected to apply, however, to other than midwing configurations. This statement also may not apply for configurations having large differences in the relative sizes of wing and fuselage.

On the assumption that wing and fuselage interference effects (for configurations similar to those tested) on tail effectiveness can be neglected, the complete tail contributions to the yawing derivatives (since the direct horizontal-tail contributions are usually small) can be calculated from the following equations, which can be derived from simple geometric considerations:

$$\left.\begin{aligned}
\left(C_{Y_r}\right)_V &= 114.6\left(\frac{l_V}{b}\cos\alpha + \frac{z_V}{b}\sin\alpha\right)\frac{S_V}{S_W}\left(C_{L_\alpha}\right)_V \\
\left(C_{n_r}\right)_V &= -114.6\left(\frac{l_V}{b}\cos\alpha + \frac{z_V}{b}\sin\alpha\right)^2\frac{S_V}{S_W}\left(C_{L_\alpha}\right)_V \\
\left(C_{l_r}\right)_V &= 114.6\left(\frac{l_V}{b}\cos\alpha + \frac{z_V}{b}\sin\alpha\right)\left(\frac{z_V}{b}\cos\alpha - \frac{l_V}{b}\sin\alpha\right)\frac{S_V}{S_W}\left(C_{L_\alpha}\right)_V
\end{aligned}\right\} \quad (2)$$

For the usual conditions, where l_V is large compared to z_V and the angle-of-attack range under consideration does not extend beyond about 20°, the following simplified equations are sufficiently accurate:

$$\left.\begin{aligned}
\left(C_{Y_r}\right)_V &= 114.6\,\frac{l_V}{b}\,\frac{S_V}{S_W}\left(C_{L_\alpha}\right)_V \\
\left(C_{n_r}\right)_V &= -114.6\left(\frac{l_V}{b}\right)^2\frac{S_V}{S_W}\left(C_{L_\alpha}\right)_V \\
\left(C_{l_r}\right)_V &= 114.6\left(\frac{z_V}{b}-\frac{l_V}{b}\sin\alpha\right)\frac{l_V}{b}\,\frac{S_V}{S_W}\left(C_{L_\alpha}\right)_V
\end{aligned}\right\} \qquad (3)$$

The tail increments $\left(C_{Y_r}\right)_V$ and $\left(C_{n_r}\right)_V$ at $\alpha = 0^\circ$ were determined from the experimental data for the vertical-tail configurations tested (horizontal tail off) and are presented in figure 20 plotted against $\frac{l_V}{b}\frac{S_V}{S_W}$ and $\left(\frac{l_V}{b}\right)^2\frac{S_V}{S_W}$, respectively. Also in the figure the variations of these increments calculated by equations (2) are indicated by a dashed line. The calculations were made using a value of $\left(C_{L_\alpha}\right)_V$ based on an effective aspect ratio A_e equal to 1.0, which was the geometric aspect ratio of the vertical tails. The good agreement between the calculated variations and the experimental values indicates little end-plate effect of the fuselages. The results obtained in static-stability tests (reference 1), however, showed that the fuselage increased the effective aspect ratio of the vertical tail by an average of about 25 percent. The effect of the fuselage in sideslip might be expected to be different from the effect in curved flight because in sideslip the free-stream angularity relative to the fuselage is constant along the fuselage length; whereas in curved flight the direction of flow varies along the fuselage and, therefore, the influence of the fuselage on the tail should be considerably different for the two conditions. The small differences of the wing-on and wing-off values shown in figure 20 and in subsequent figures indicate only a small effect of wing-fuselage interference on the vertical-tail effectiveness at 0° angle of attack. Figure 21 corresponds to figure 20 and shows the experimental increments of $\left(C_{l_r}\right)_V$ and $\frac{\partial\left(C_{l_r}\right)_V}{\partial\alpha}$ plotted

against $\frac{l_V}{b}\frac{z_V}{b}\frac{S_V}{S_W}$ and $\left(\frac{l_V}{b}\right)^2\frac{S_V}{S_W}$, respectively, for the configurations with horizontal tail off. The values obtained are rather small, as expected, and the values calculated are in fairly good agreement with the experimental points.

The effect of the horizontal tail on the tail contributions is shown in figure 22, which presents the experimental increments $(C_{Y_r})_V$ and $(C_{n_r})_V$ (obtained from figs. 13 and 14) of the vertical-tail and horizontal-tail combinations tested. It should be noted that, when a horizontal tail is used, the tail contribution is considered to consist of the effect of the complete tail group. A line faired through the experimental values of $(C_{Y_r})_V$ was found to correspond to a value of $(C_{L_\alpha})_V$ (with the use of equations (3)) such that an increase in effective aspect ratio from 1.00 to 1.43 was indicated (according to reference 6). This increase is attributed to the end-plate effect of the horizontal-tail - fuselage combination on the vertical tail. The calculated variation of $(C_{n_r})_V$ computed with the use of the value of $(C_{L_\alpha})_V$ determined in this manner for 0° angle of attack shows good agreement with the experimental values as was, of course, expected. The increase in effective aspect ratio obtained is about equal to the end-plate effect of a fuselage and horizontal-tail combination as determined from static-stability tests (reference 2). For purposes of comparison, the calculated variation of $(C_{Y_r})_V$ and $(C_{n_r})_V$ for a vertical tail of effective aspect ratio of 1.0 is also shown in this figure.

The foregoing general procedure was followed in computing the tail contributions for one wing-fuselage combination for the slat-extended condition. The results are plotted in figure 23. The calculated variation of $(C_{Y_r})_V$ and $(C_{n_r})_V$, based on a value of $(C_{L_\alpha})_V$ corresponding to $A_e = 1.00$, was plotted in the figure and shows fairly good agreement with the experimental results for the horizontal-tail-off configuration. A line was faired through the experimental points for the configuration with horizontal tail on and was found to correspond to a value of $(C_{L_\alpha})_V$ which results in a value of A_e of 1.45 which is to all practical purposes the same as that obtained with the plain wing and indicates little effect of wing slat on the tail effectiveness at 0° angle of attack. From the foregoing discussion, it appears that for the horizontal-tail-off configurations considered, the geometric aspect ratio of the vertical tail is accurate enough to be used to estimate the vertical-tail lift-curve slope at 0° angle of attack of the model in yawing flow. For the models with horizontal tail located at the base of the vertical tail, the

effective aspect ratio as determined at 0° angle of attack from static-stability tests of similar configurations is of sufficient accuracy to be used in estimates of the vertical-tail lift-curve slope at 0° angle of attack of the model in yawing flow.

The values of $(C_{L_\alpha})_V$ at 0° angle of attack of the model, corresponding to $A_e = 1.00$ and 1.45, were therefore used to calculate the variation of $(C_{Y_r})_V$, $(C_{n_r})_V$, and $(C_{l_r})_V$ with angle of attack. The calculated values are compared with the experimental values in figures 24 to 26. Also presented in the figures are the variations with angle of attack of $(C_{Y_r})_V$, $(C_{n_r})_V$, and $(C_{l_r})_V$ calculated by substituting $(C_{Y_\psi})_V$ for $\frac{S_V}{S_W}(C_{L_\alpha})_V$ in equations (2). The values of $(C_{Y_\psi})_V$ used in the computations are the experimental values for each angle of attack as determined for the configurations considered in reference 1. The values calculated by both methods agree reasonably well with the experimental results in the low angle-of-attack range. In general, the agreement is poorer at high angles of attack. With the exception of the results for the short-fuselage configurations, the values calculated with the use of measured values of $(C_{Y_\psi})_V$ are not in as good agreement through the range of angle of attack up to maximum lift as those obtained with the use of calculated values of $(C_{l_\alpha})_V$ at 0° angle of attack of the model. The results discussed indicate that values of $(C_{L_\alpha})_V$ at 0° angle of attack of the model can be estimated fairly accurately by available procedures and would give reasonably reliable estimates of tail contributions to C_{Y_r}, C_{n_r}, and C_{l_r} for most of the angle-of-attack range for the wing-on condition. As was mentioned before, the results presented herein are for midwing configurations and may not apply to high- or low-wing configurations. These results also may not apply for configurations having a wing which is small relative to the fuselage.

CONCLUSIONS

The results of an investigation to determine the effect of vertical-tail area and tail length on the yawing stability characteristics of models having an aspect-ratio-4 wing with quarter-chord line swept back 45° indicated the following conclusions:

1. The effects of wing-fuselage interference for the midwing arrangements tested were small over most of the angle-of-attack range.

2. Although rather large interference effects on vertical-tail effectiveness appeared to be produced by the fuselage and by the wing at moderate and high angles of attack, these interference effects tended to cancel each other and, therefore, had little effect on tail effectiveness of the complete configurations tested.

3. The fuselage alone had little effect on the effective aspect ratio of the vertical tail at 0° angle of attack in the yawing condition. Addition of the horizontal tail at the base of the vertical tail produced an increase in effective aspect ratio nearly equal to that obtained in static-stability tests for a fuselage - horizontal-tail combination.

4. For the configurations tested, the tail contributions to the yawing derivatives were estimated fairly accurately for most of the angle-of-attack range by available procedures. The estimates based on the value of the tail lift-curve slope at 0° angle of attack gave, for the medium and for the long tail lengths, somewhat better results up to the angle of attack of maximum lift than calculations based on the measured values of lateral force resulting from yaw angle.

5. A full-span wing slat had very little effect on the tail effectiveness at 0° angle of attack.

Langley Aeronautical Laboratory
National Advisory Committee for Aeronautics
Langley Field, Va., February 6, 1951

REFERENCES

1. Queijo, M. J., and Wolhart, Walter D.: Experimental Investigation of the Effect of Vertical-Tail Size and Length and of Fuselage Shape and Length on the Static Lateral Stability Characteristics of a Model with 45° Sweptback Wing and Tail Surfaces. NACA TN 2168, 1950.

2. Brewer, Jack D., and Lichtenstein, Jacob H.: Effect of Horizontal Tail on Low-Speed Static Lateral Stability Characteristics of a Model Having 45° Sweptback Wing and Tail Surfaces. NACA TN 2010, 1950.

3. Recant, Isidore G., and Wallace, Arthur R.: Wind-Tunnel Investigation of Effect of Yaw on Lateral-Stability Characteristics. III - Symmetrically Tapered Wing at Various Positions on Circular Fuselage with and without a Vertical Tail. NACA TN 825, 1941.

4. Goodman, Alex, and Fisher, Lewis R.: Investigation at Low Speeds of the Effect of Aspect Ratio and Sweep on Rolling Stability Derivatives of Untapered Wings. NACA Rep. 968, 1950.

5. Toll, Thomas A., and Queijo, M. J.: Approximate Relations and Charts for Low-Speed Stability Derivatives of Swept Wings. NACA TN 1581, 1948.

6. DeYoung, John: Theoretical Additional Span Loading Characteristics of Wings with Arbitrary Sweep, Aspect Ratio, and Taper Ratio. NACA TN 1491, 1947.

TABLE I.- FUSELAGE COORDINATES

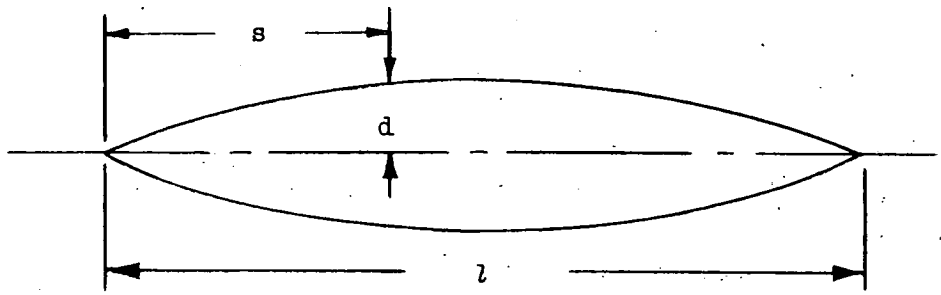

s/l	d/l		
	Fuselage 1	Fuselage 2	Fuselage 3
0	0	0	0
.025	.010	.007	.005
.050	.020	.014	.010
.075	.029	.021	.014
.100	.037	.027	.018
.125	.045	.033	.022
.150	.052	.039	.026
.200	.065	.048	.032
.250	.076	.057	.038
.30	.085	.063	.042
.35	.091	.068	.046
.40	.096	.072	.048
.45	.099	.074	.049
.50	.100	.075	.050
.55	.099	.074	.049
.60	.096	.072	.048
.65	.091	.068	.046
.70	.085	.063	.042
.75	.076	.057	.038
.80	.065	.048	.032
.85	.052	.039	.026
.90	.037	.027	.018
.95	.020	.014	.010
1.00	0	0	0

TABLE II.- PERTINENT GEOMETRIC CHARACTERISTICS OF MODEL

Wing:			
Aspect ratio			4.0
Taper ratio			0.6
Quarter-chord sweep angle, deg			45
Dihedral angle, deg			0
Twist, deg			0
Incidence, deg			0
NACA airfoil section			65A008
Area, sq in.			324
Span, in.			36.0
Mean aerodynamic chord, in.			9.19
Fuselage:	F_1	F_2	F_3
Length, in.	30	40	60
Fineness ratio	5.00	6.67	10.00
Volume, cu in.	461	605	909
Tail length, in. (all tails)	12.5	16.7	25.1
Ratio of tail length to wing span (all tails)	0.347	0.464	0.697
Side area, sq in.	120	160	240
Vertical tail:	V_1	V_2	V_3
Aspect ratio	1.0	1.0	1.0
Taper ratio	0.6	0.6	0.6
Quarter-chord sweep angle, deg	45	45	45
NACA airfoil section	65A008	65A008	65A008
Area, sq in.	24.3	48.6	72.9
Span, in.	4.9	7.0	8.5
Mean aerodynamic chord, in.	5.0	7.1	8.7
Ratio of tail area to wing area	0.075	0.150	0.225
Horizontal tail:			
Aspect ratio			2.0
Taper ratio			0.6
Quarter-chord sweep angle, deg			45
NACA airfoil section			65A008
Area, sq in.			64.80
Span, in.			16.10
Mean aerodynamic chord, in.			4.11
Ratio of tail area to wing area			0.20

TABLE III.- CONFIGURATIONS INVESTIGATED

Wing off		Wing on	
Configuration (a)	Figure	Configuration (a)	Figure
----------	------	W	6, 7, 8
----------	------	W_S	6, 7, 8
----------	------	$W + F_1$	10
----------	------	$W + F_1 + V_1$	10
----------	------	$W + F_1 + V_2$	10
----------	------	$W + F_1 + V_3$	10
F_2	9	$W + F_2$	11
$F_2 + V_1$	9	$W + F_2 + V_1$	11
$F_2 + V_2$	9	$W + F_2 + V_2$	11
$F_2 + V_3$	9	$W + F_2 + V_3$	11
----------	------	$W + F_3$	12
----------	------	$W + F_3 + V_1$	12
----------	------	$W + F_3 + V_2$	12
----------	------	$W + F_3 + V_3$	12
$F_2 + H + V_1$	13	$W + F_2 + H + V_1$	14
$F_2 + H + V_2$	13	$W + F_2 + H + V_2$	14
$F_2 + H + V_3$	13	$W + F_2 + H + V_3$	14
----------	------	$W_S + F_2$	15
----------	------	$W_S + F_2 + V_1$	15
----------	------	$W_S + F_2 + V_2$	15
----------	------	$W_S + F_2 + V_3$	15
----------	------	$W_S + F_2 + H + V_1$	16
----------	------	$W_S + F_2 + H + V_2$	16
----------	------	$W_S + F_2 + H + V_3$	16

[a]Notation (for details, see table II and figs. 2 to 4):

W wing; with subscript S, wing with slat
F fuselage
V vertical tail
H horizontal tail

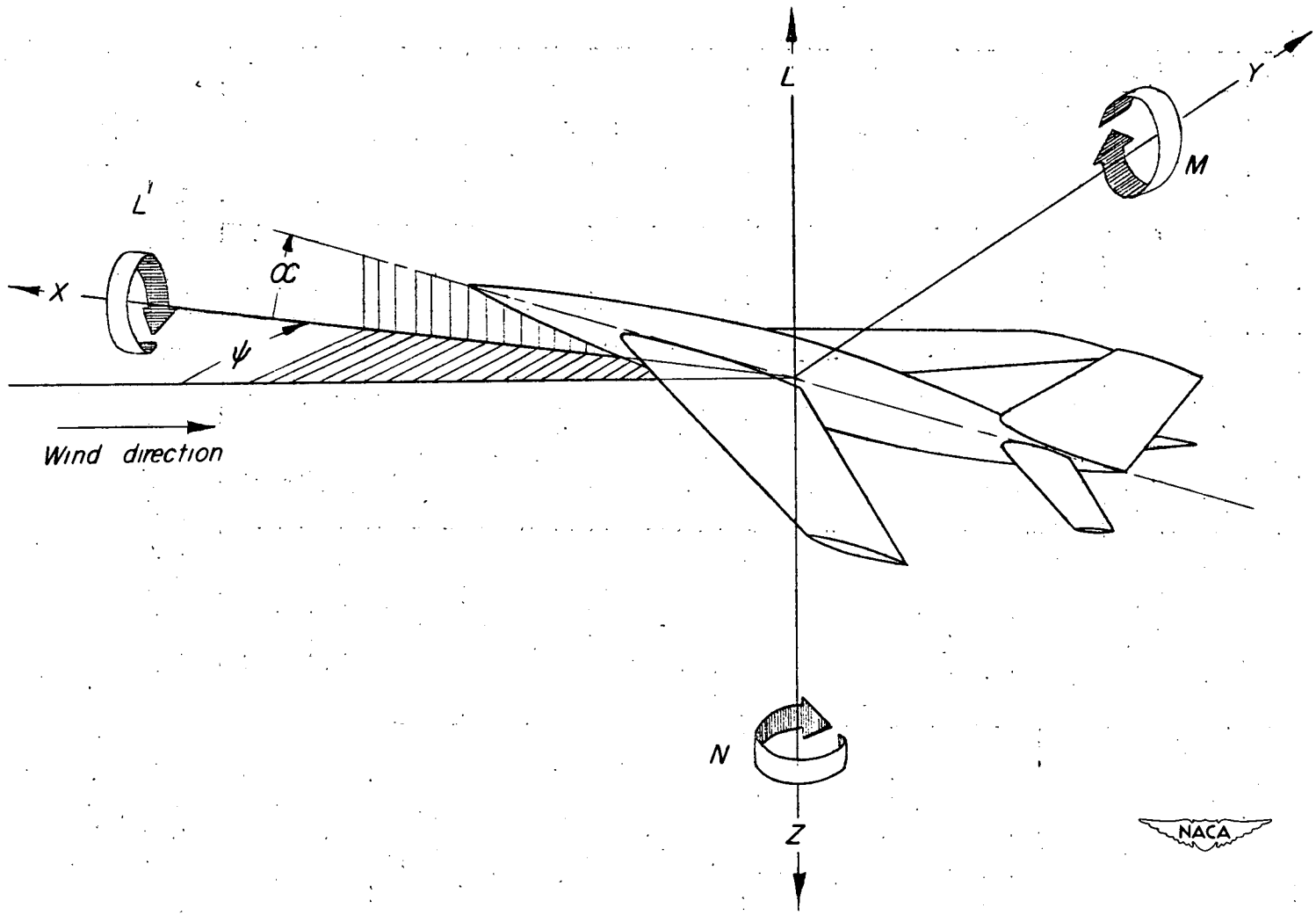

Figure 1.- System of axes used. Arrows indicate positive direction of angles, forces, and moments.

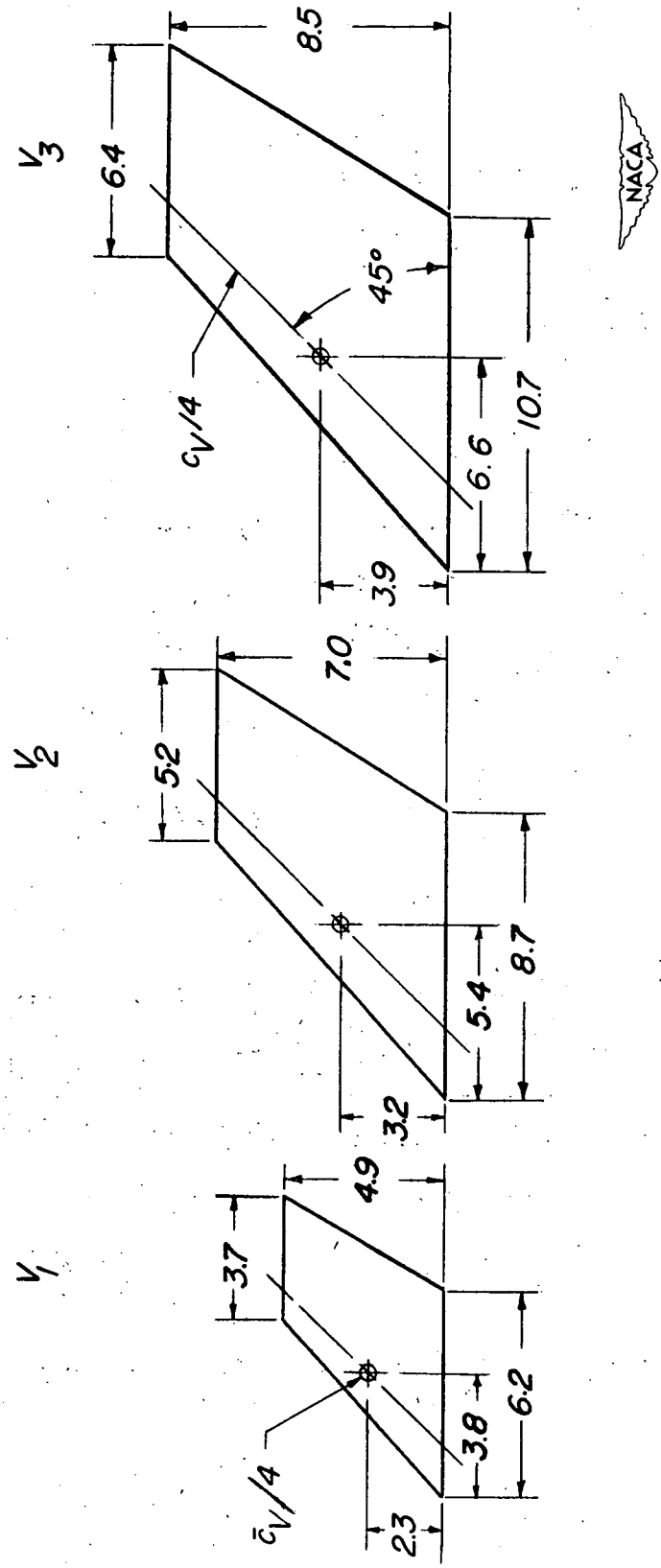

Figure 2.- Dimensions of vertical tails tested. All dimensions are in inches.

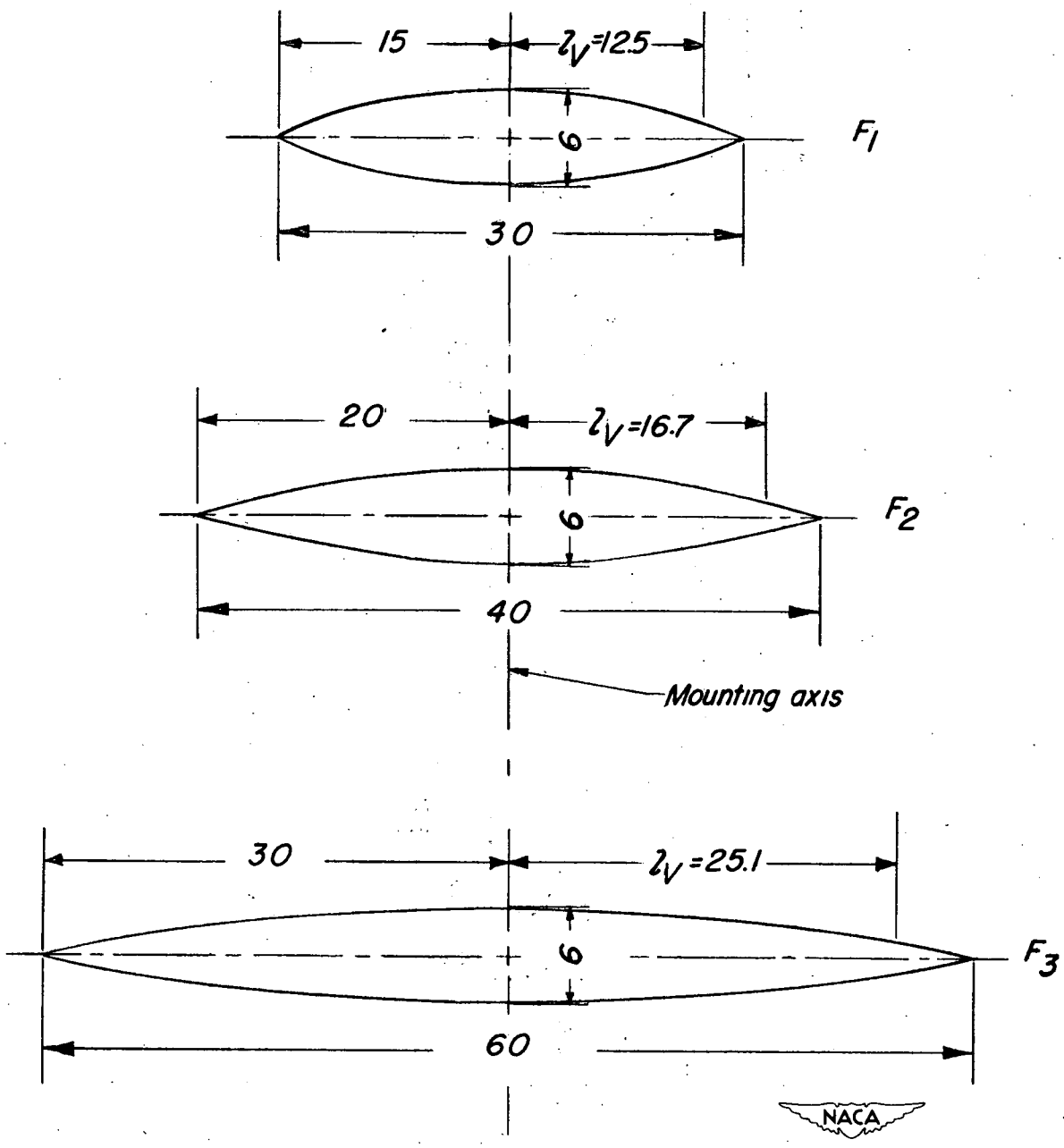

Figure 3.- Dimensions of fuselages tested; profile coordinates in table I. All dimensions are in inches.

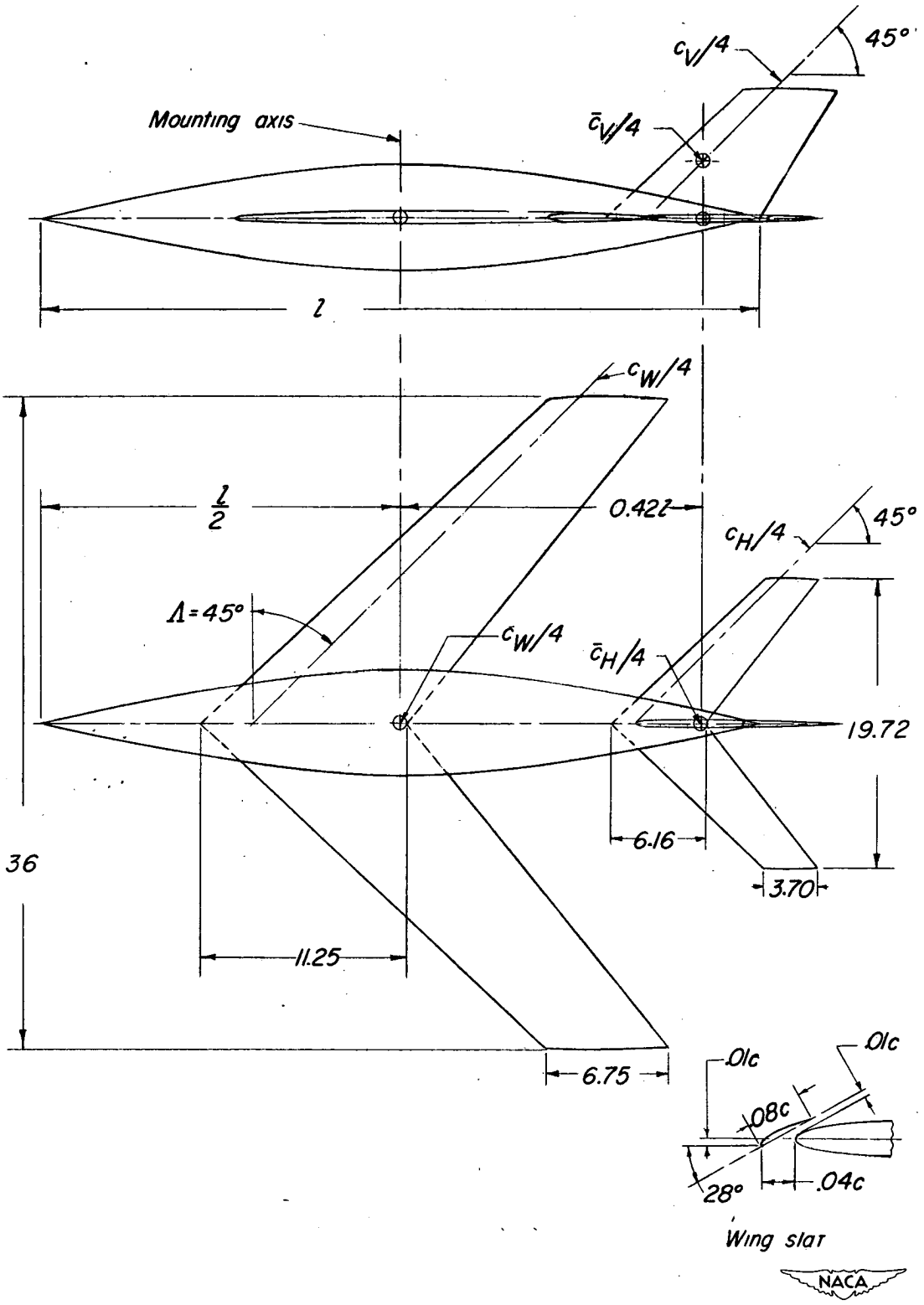

Figure 4.- Dimensions of wing, wing slat, and horizontal tail and relative location of wing and tail surfaces with respect to fuselage. All dimensions are in inches.

Page intentionally left blank

Page intentionally left blank

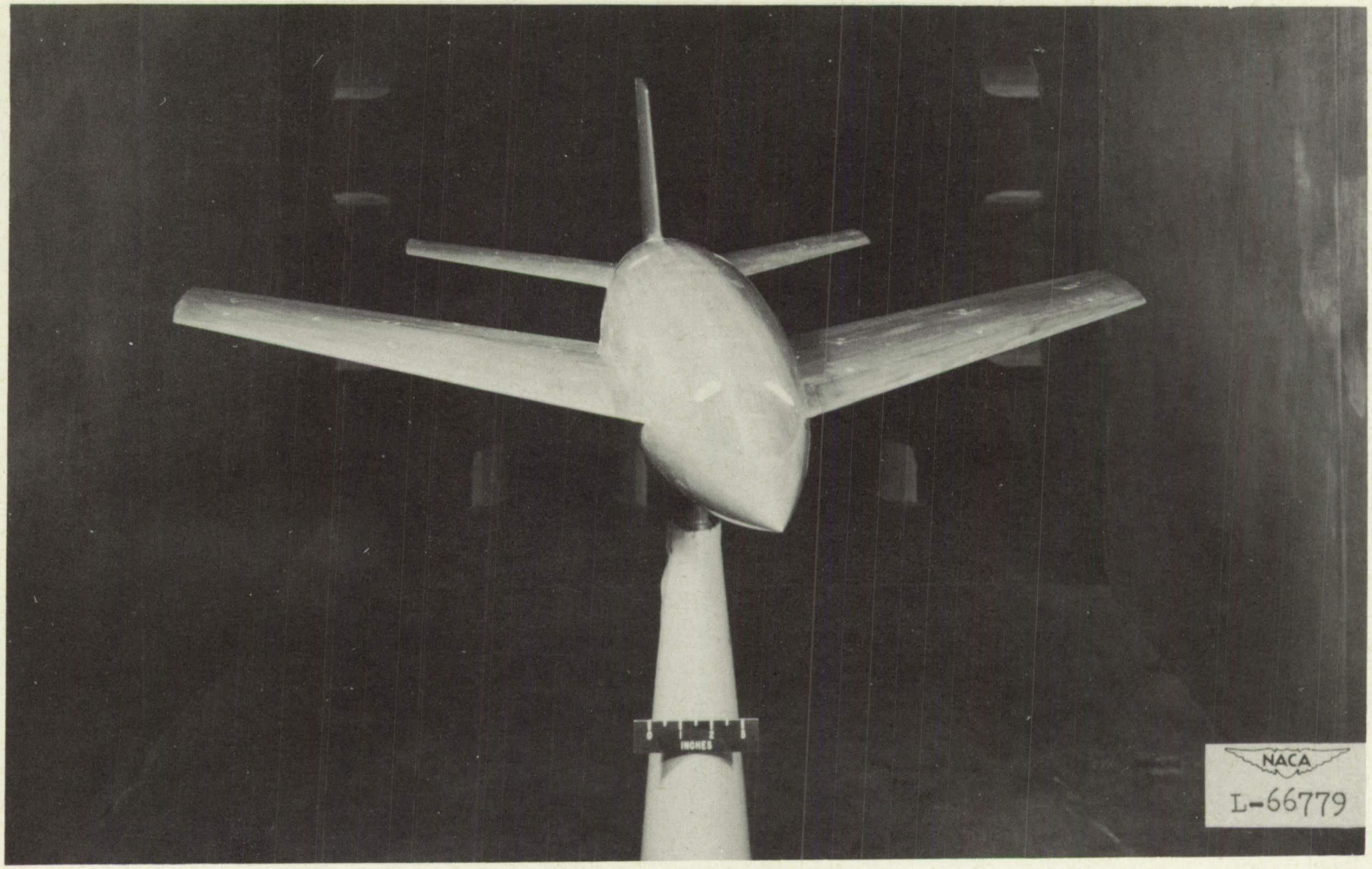

Figure 5.- View of model in Langley stability tunnel.
Configuration $W + F_2 + H + V_2$.

Page intentionally left blank

Page intentionally left blank

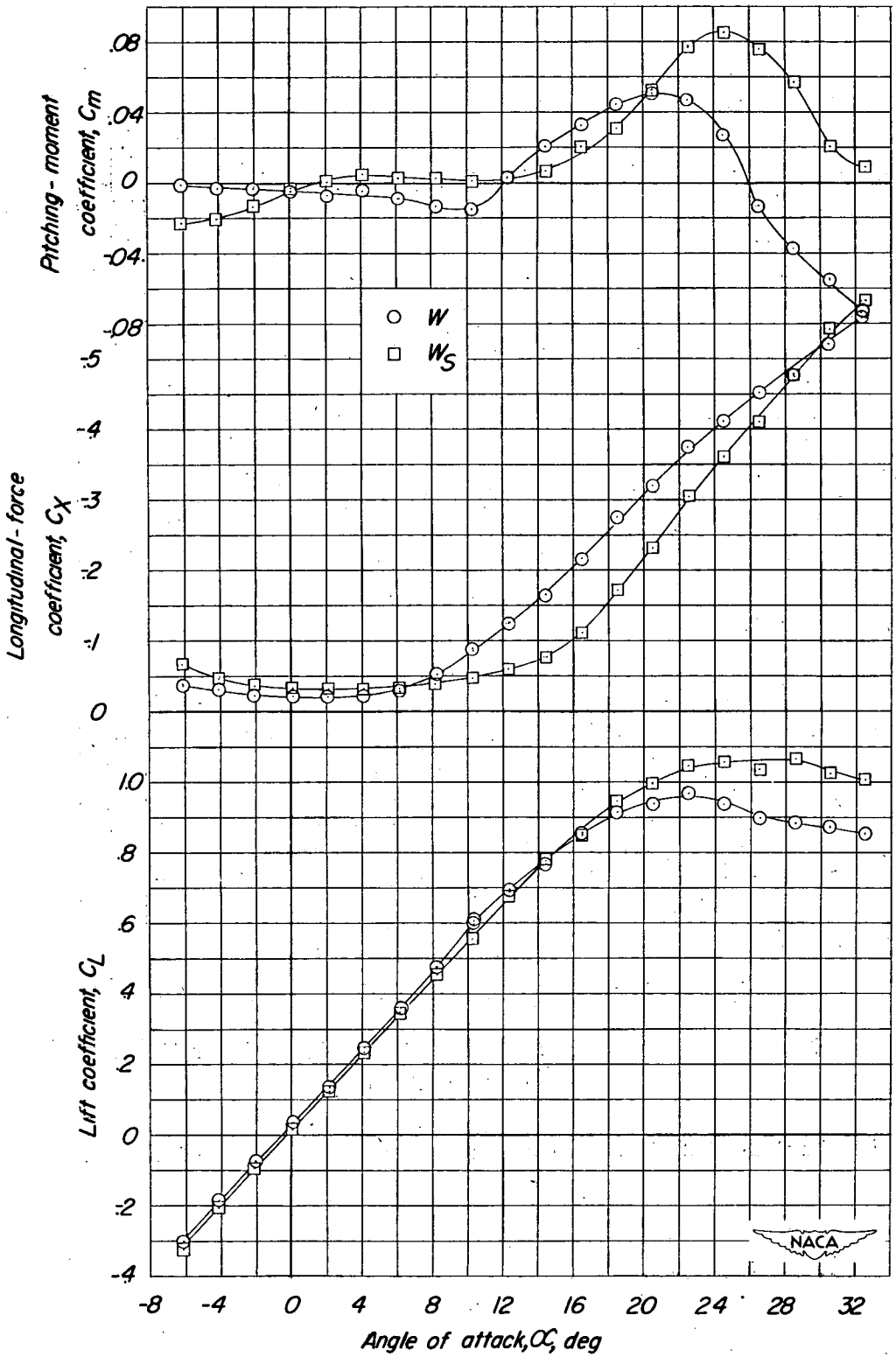

Figure 6.- Aerodynamic characteristics of wing and wing with slat.

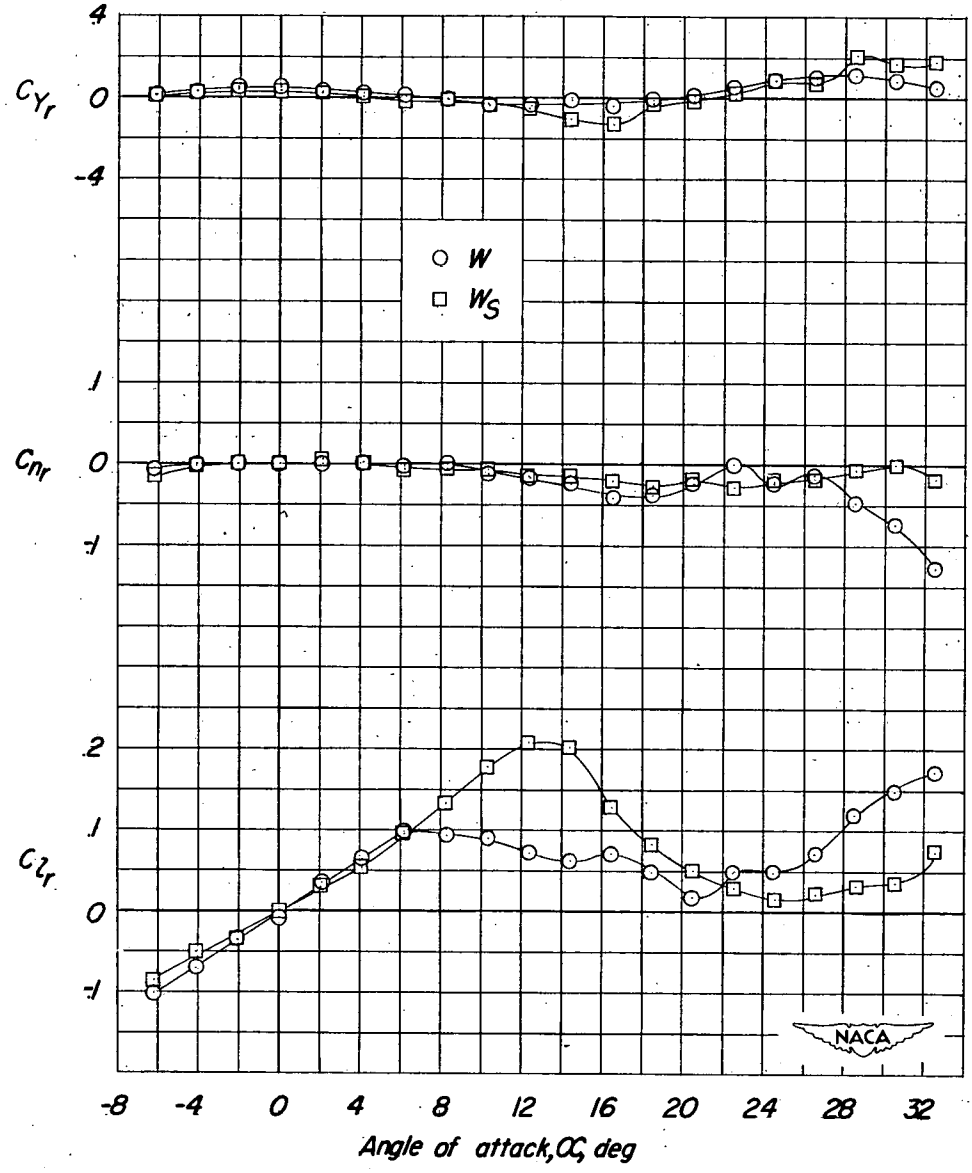

Figure 7.- Yawing stability characteristics of wing and wing with slat.

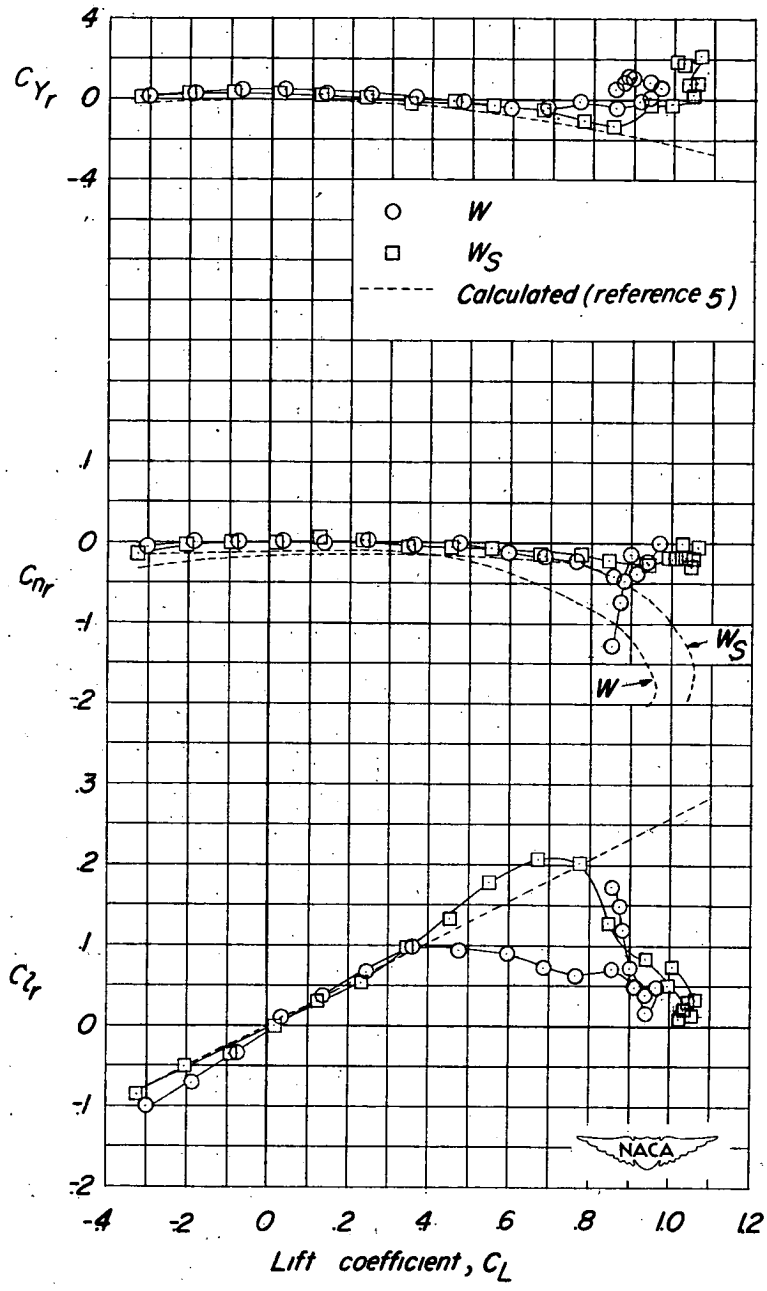

Figure 8.- Yawing stability characteristics of wing and wing with slat compared with calculated values.

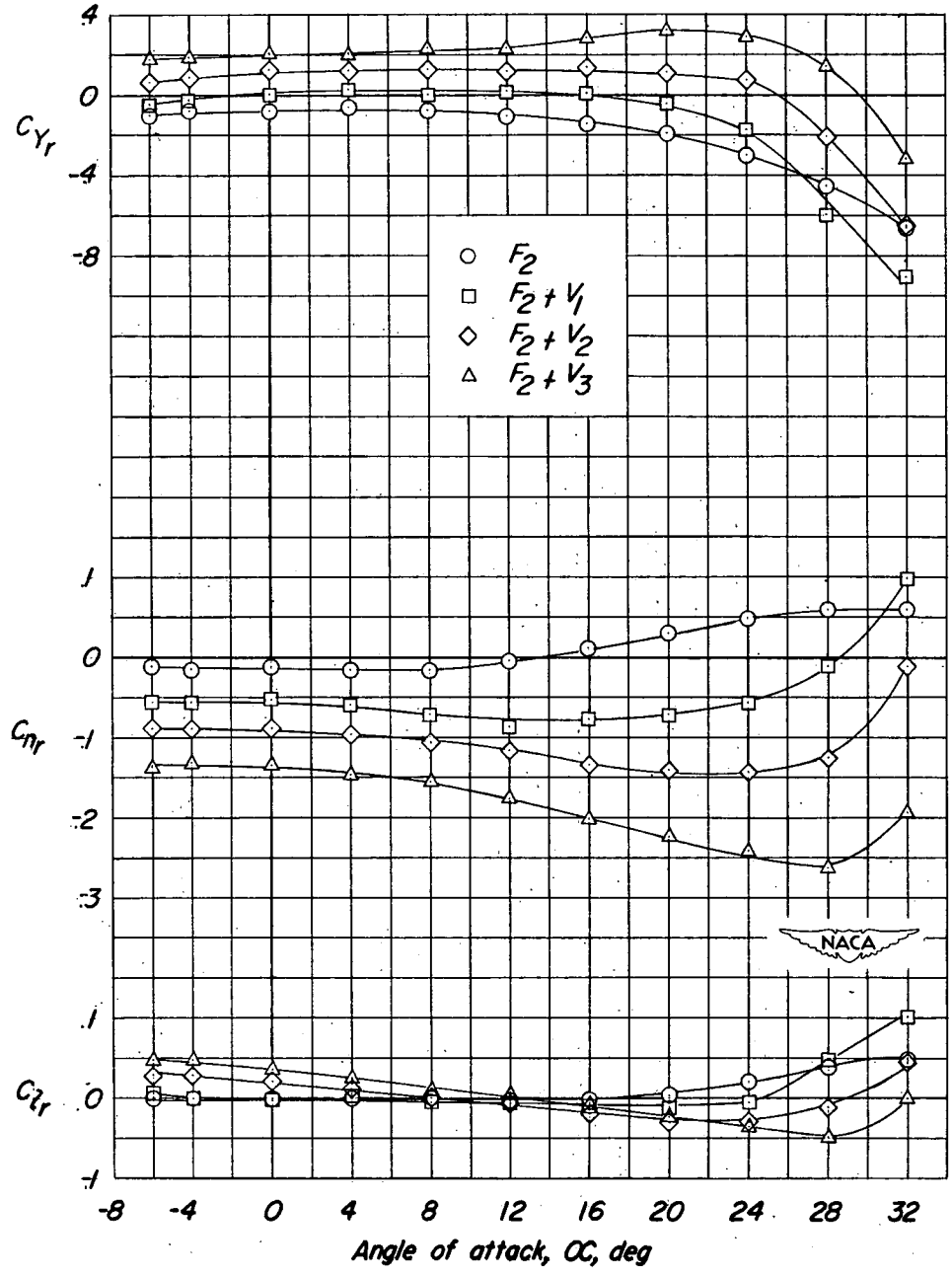

Figure 9.- Effect of vertical tail on C_{Y_r}, C_{n_r}, and C_{l_r}. Wing off; horizontal tail off; fuselage 2; $\frac{l_V}{b} = 0.464$.

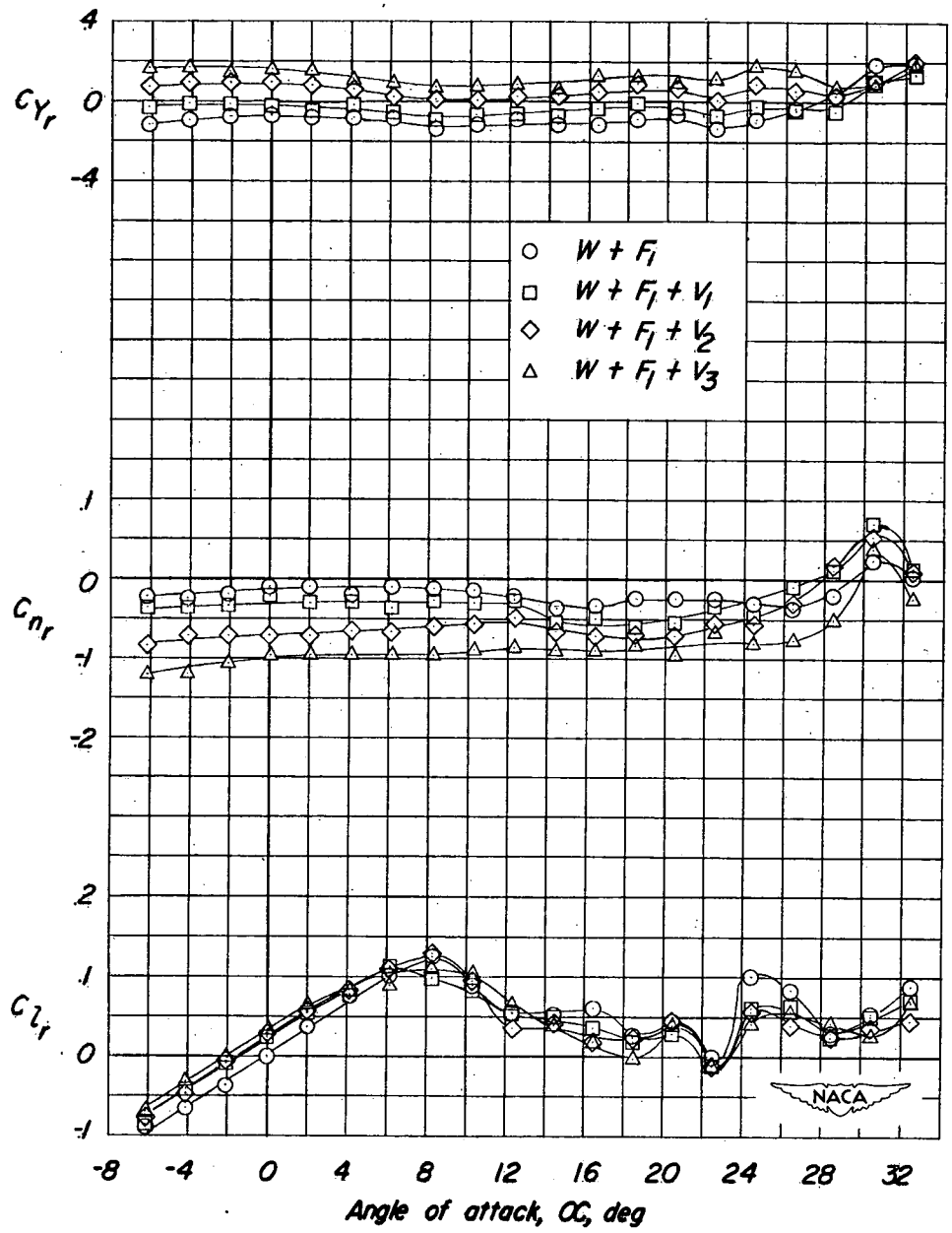

Figure 10.- Effect of vertical tail on C_{Y_r}, C_{n_r}, and C_{l_r}. Wing on; horizontal tail off; fuselage 1; $\frac{l_V}{b} = 0.347$.

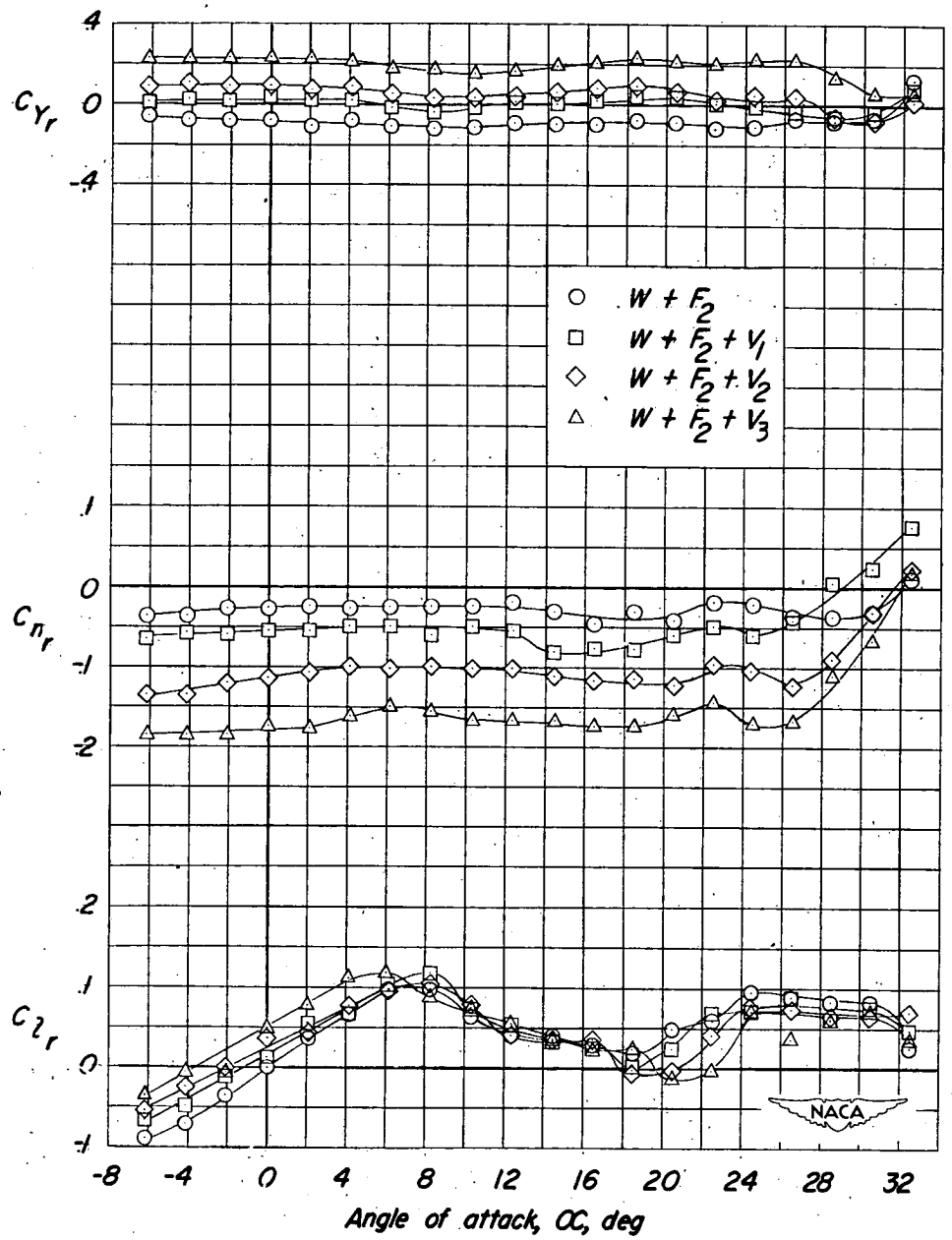

Figure 11.- Effect of vertical tail on C_{Y_r}, C_{n_r}, and C_{l_r}. Wing on; horizontal tail off; fuselage 2; $\frac{l_V}{b} = 0.464$.

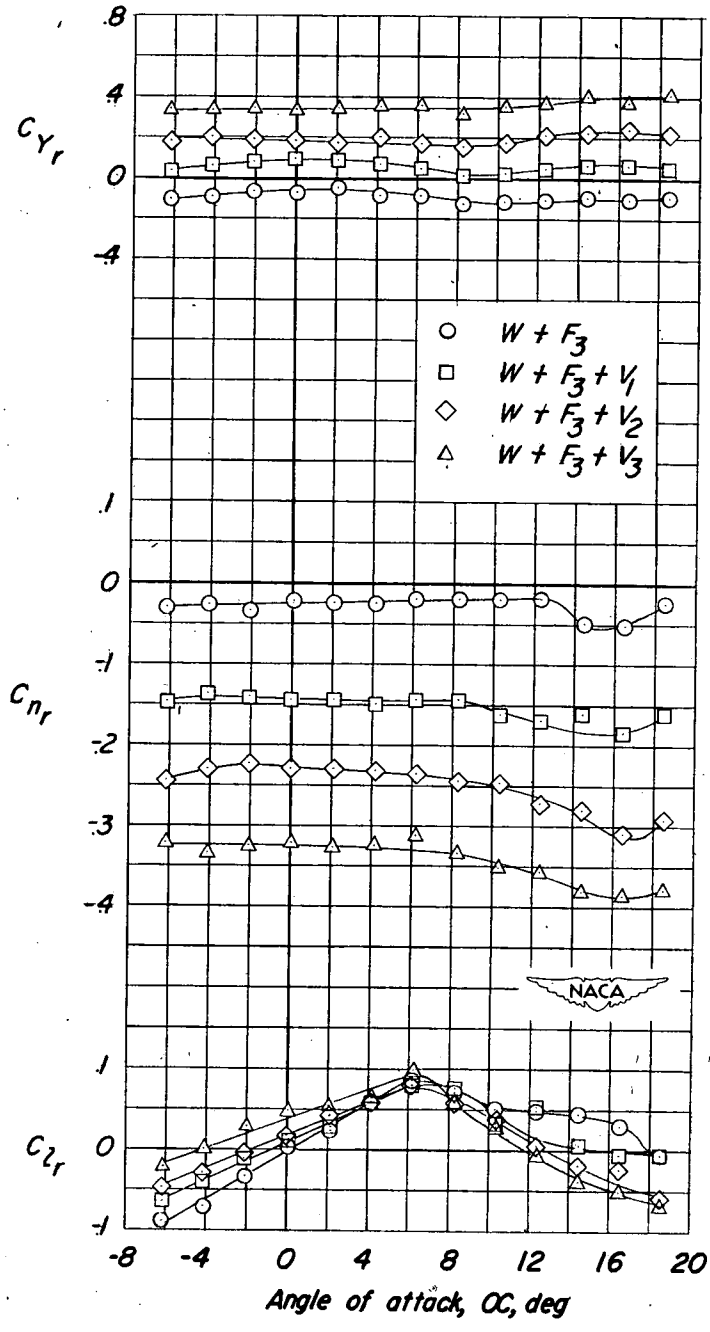

Figure 12.- Effect of vertical tail on C_{Y_r}, C_{n_r}, and C_{l_r}. Wing on; horizontal tail off; fuselage 3; $\frac{l_V}{b} = 0.697$.

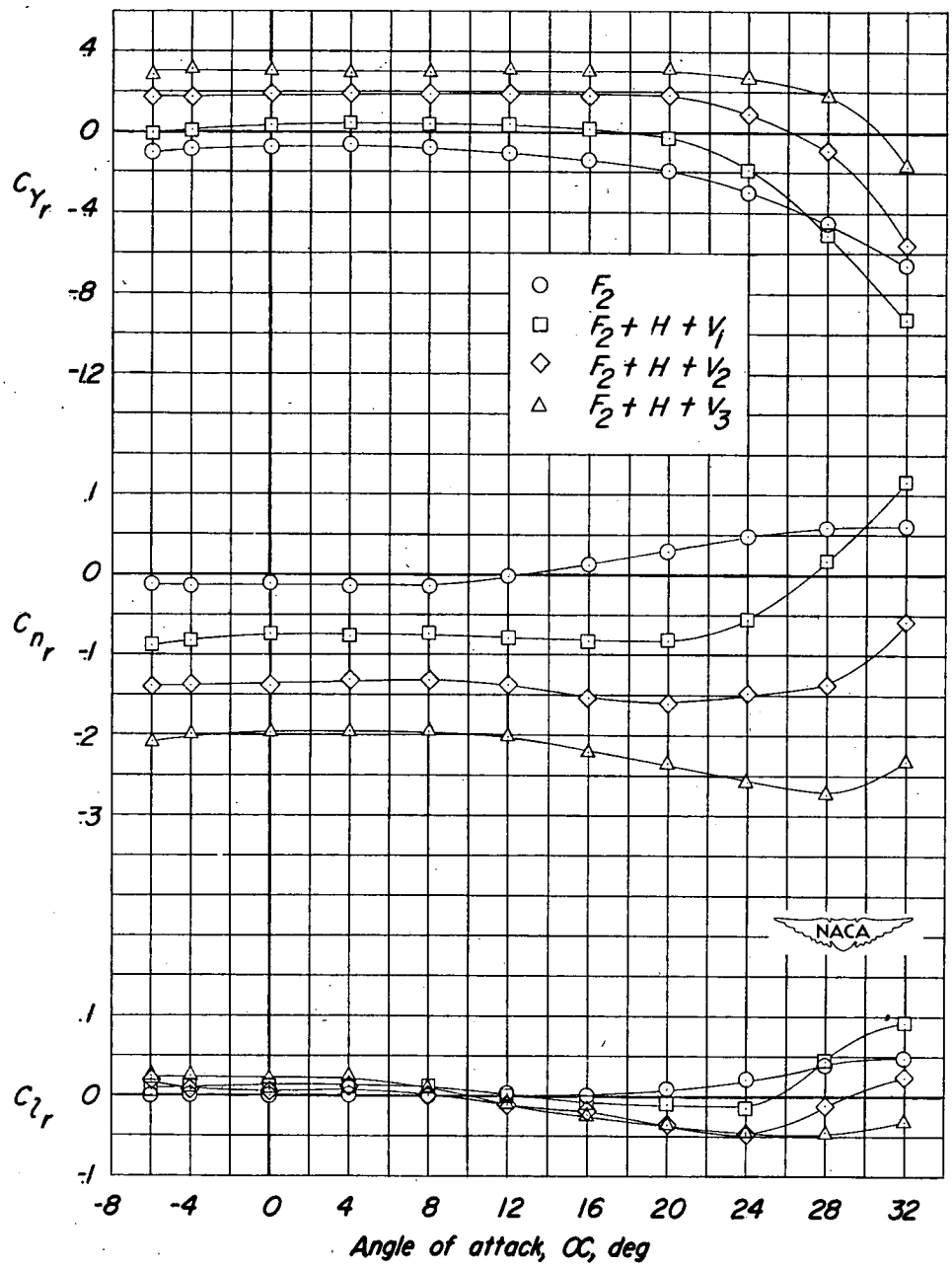

Figure 13.- Effect of vertical tail on C_{Y_r}, C_{n_r}, and C_{l_r}. Wing off; horizontal tail on; fuselage 2; $\frac{l_V}{b} = 0.464$.

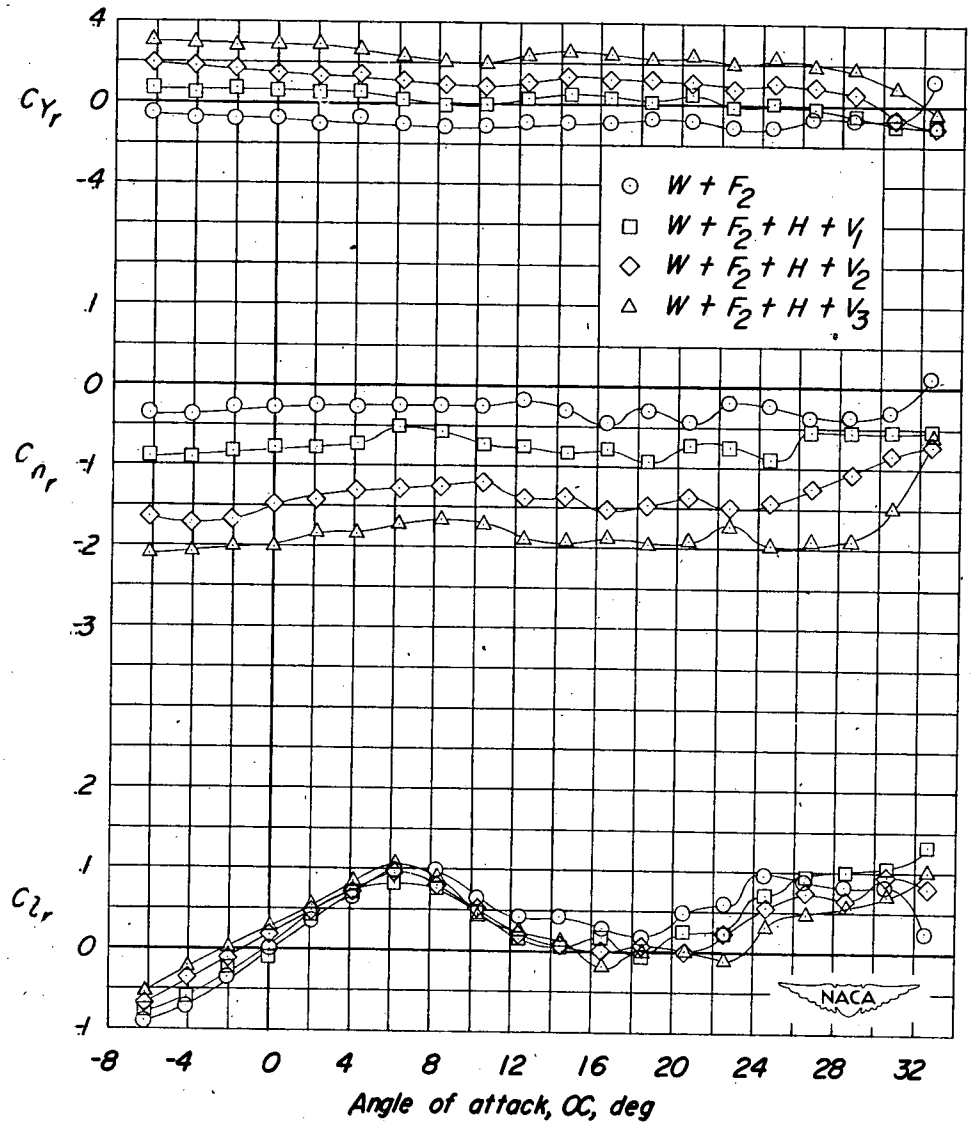

Figure 14.- Effect of vertical tail on C_{Y_r}, C_{n_r}, and C_{l_r}. Wing on; horizontal tail on; fuselage 2; $\frac{l_V}{b} = 0.464$.

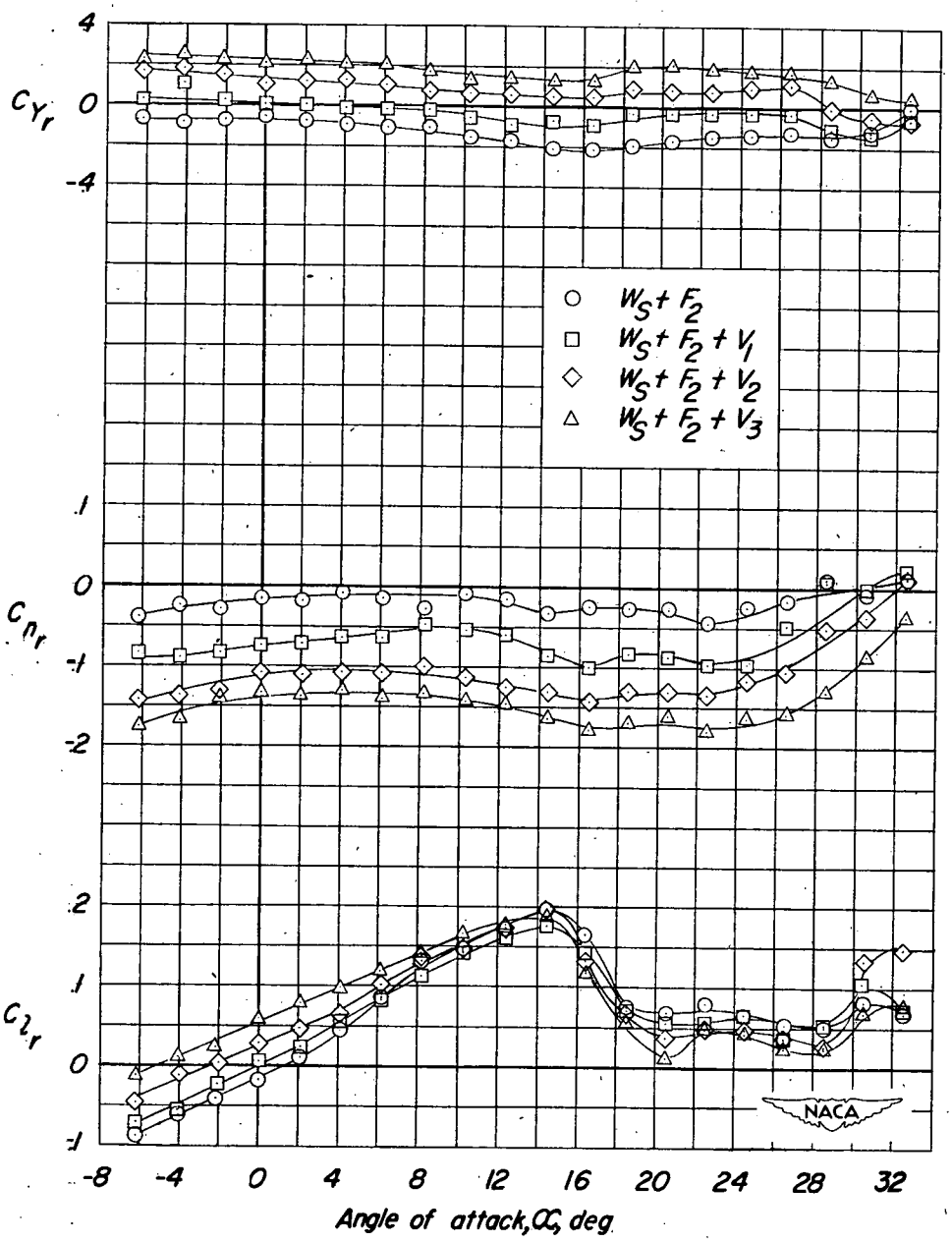

Figure 15.- Effect of vertical tail on C_{Y_r}, C_{n_r}, and C_{l_r}. Wing with slat on; horizontal tail off; fuselage 2; $\frac{l_V}{b} = 0.464$.

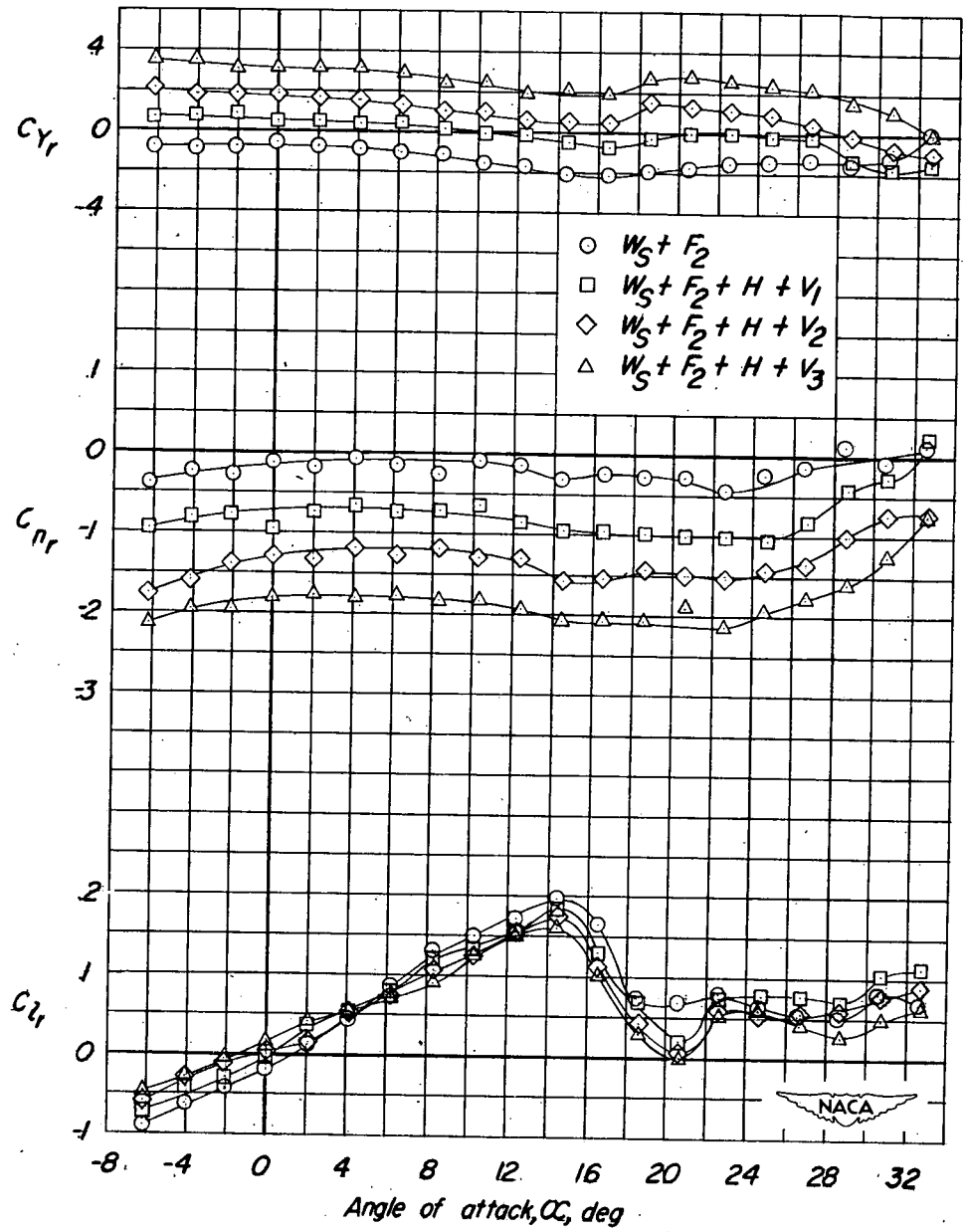

Figure 16.- Effect of vertical tail on C_{Y_r}, C_{n_r}, and C_{l_r}. Wing with slat on; horizontal tail on; fuselage 2; $\frac{l_V}{b} = 0.464$.

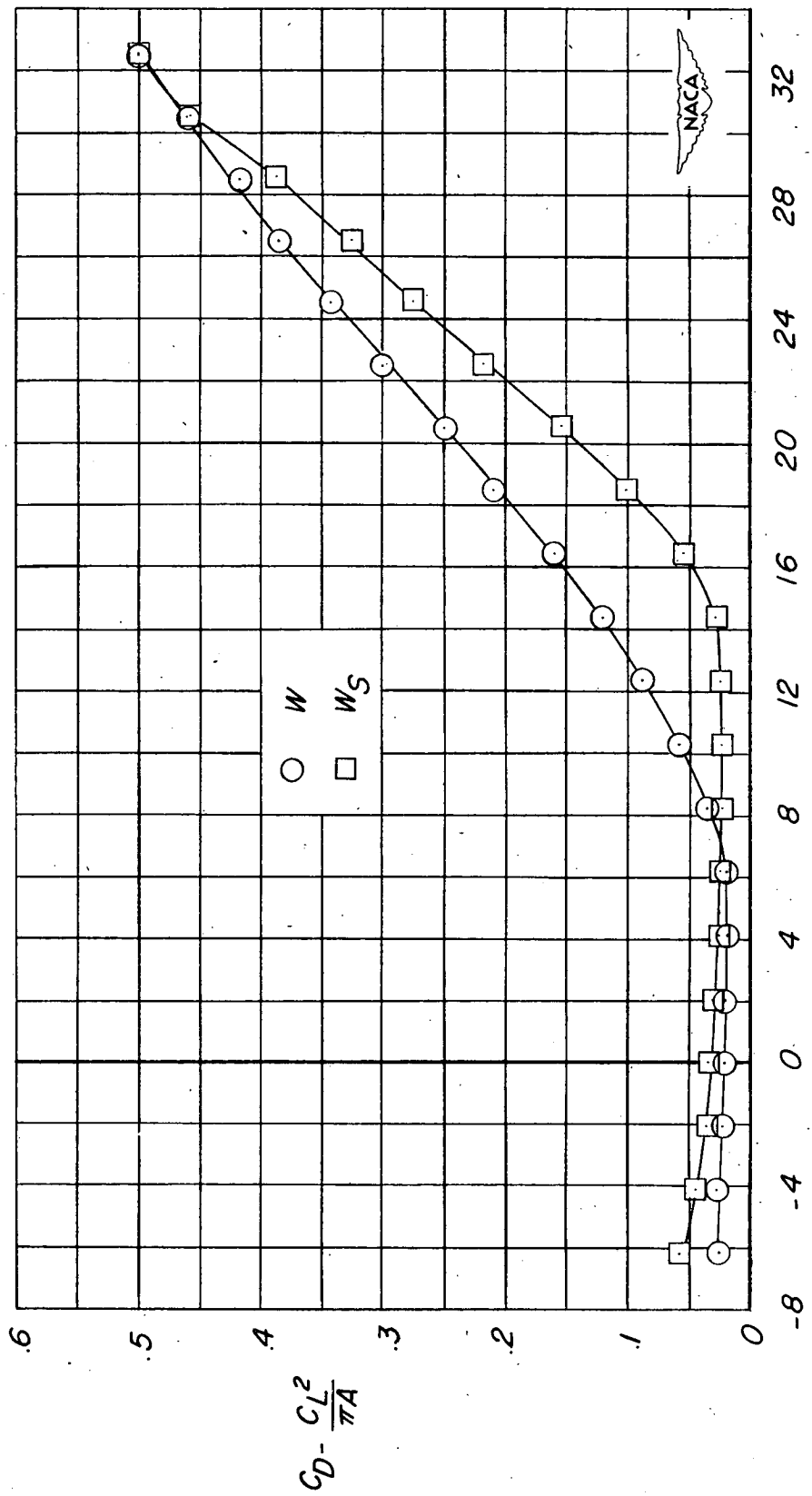

Figure 17.- Variation of the increment $C_D - \frac{C_L^2}{\pi A}$ with angle of attack for the plain wing and wing with slat.

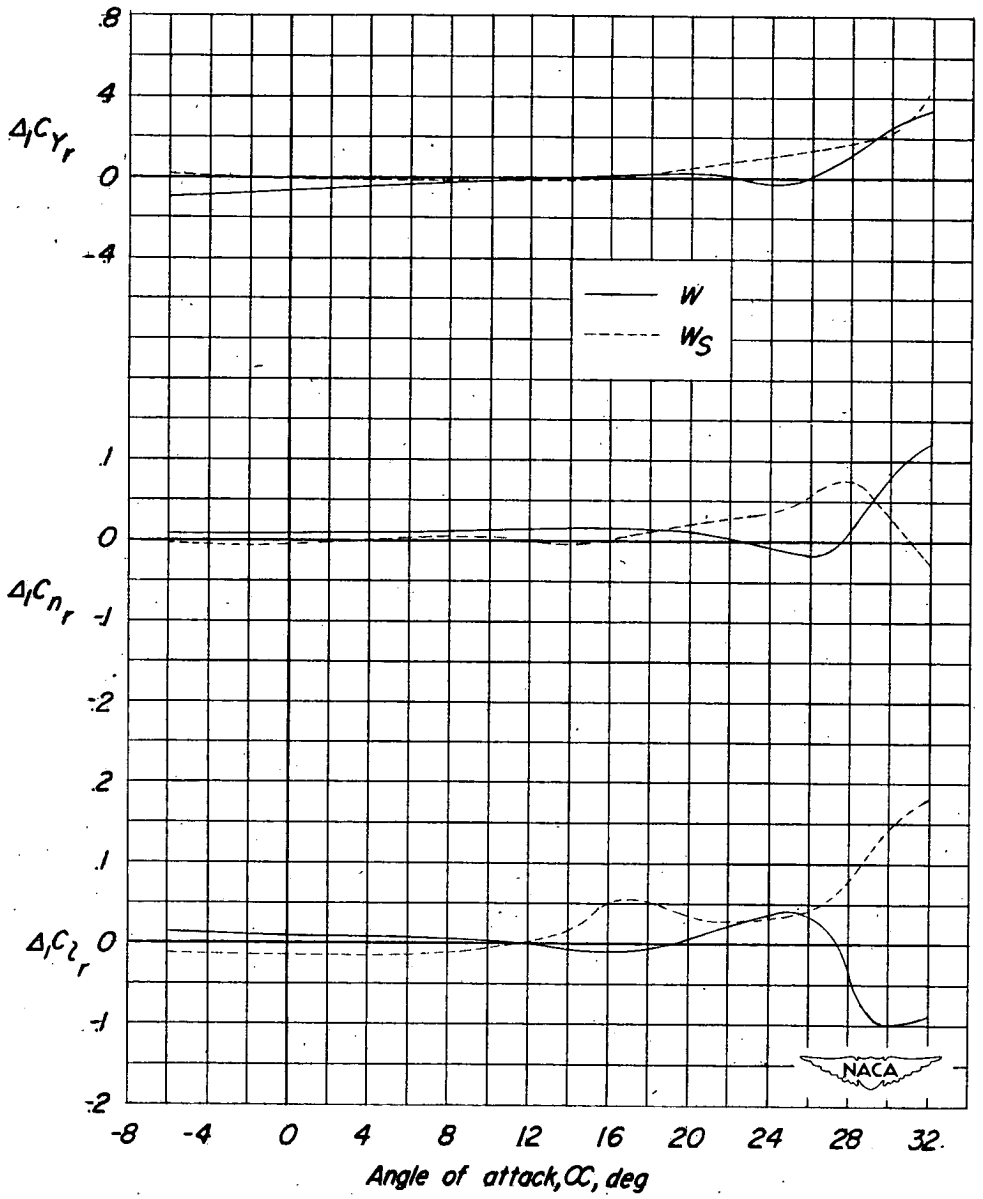

Figure 18.- Variation with angle of attack of the interference increments $\Delta_1 C_{Y_r}$, $\Delta_1 C_{n_r}$, and $\Delta_1 C_{l_r}$ for plain wing and the wing with slat.

Fuselage 2; $\frac{l_V}{b} = 0.464$.

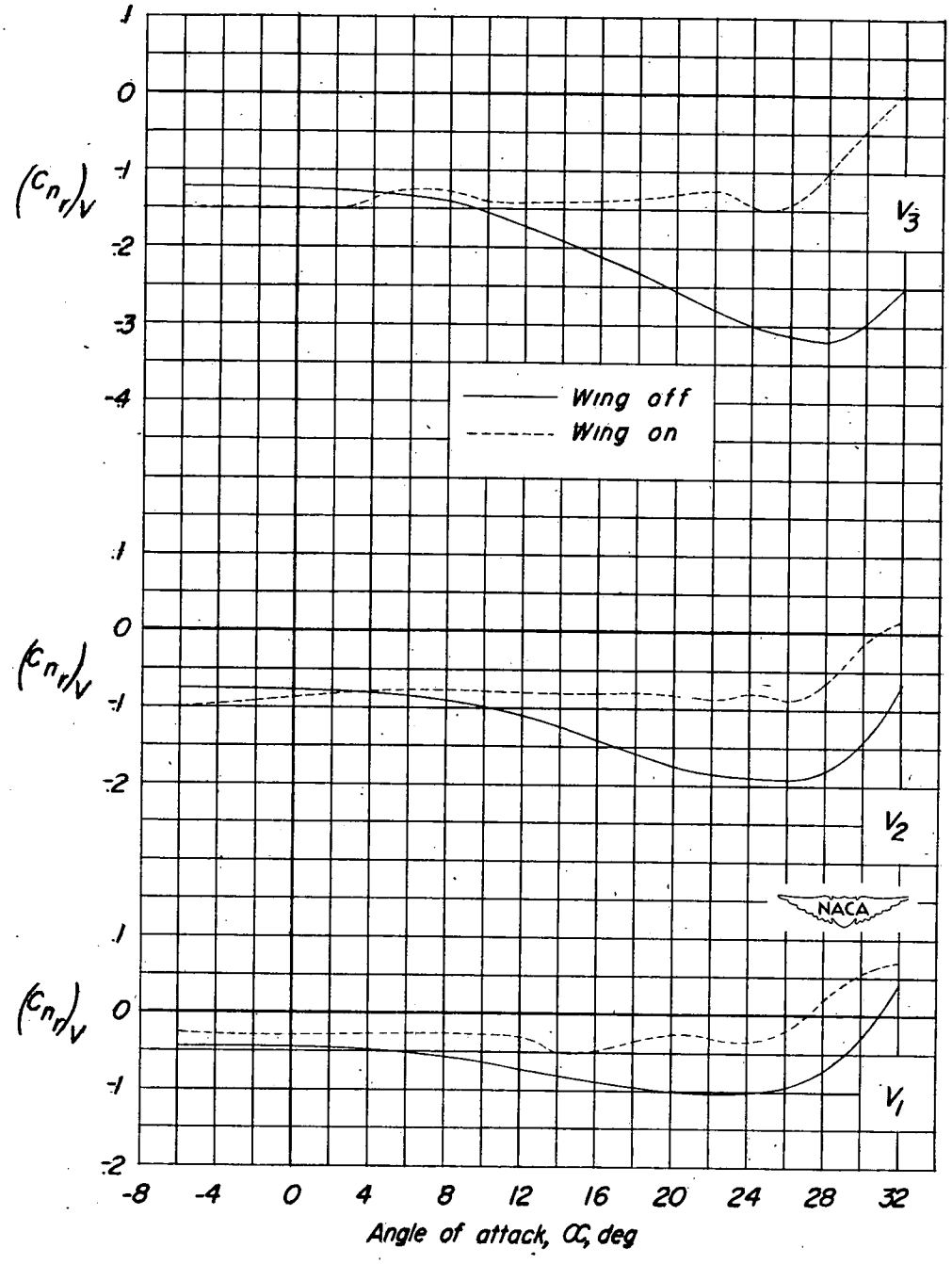

(a) Horizontal tail off.

Figure 19.- Variation with angle of attack of the wing-on and wing-off increment of $\left(C_{n_r}\right)_V$. Fuselage 2; $\frac{l_V}{b} = 0.464$.

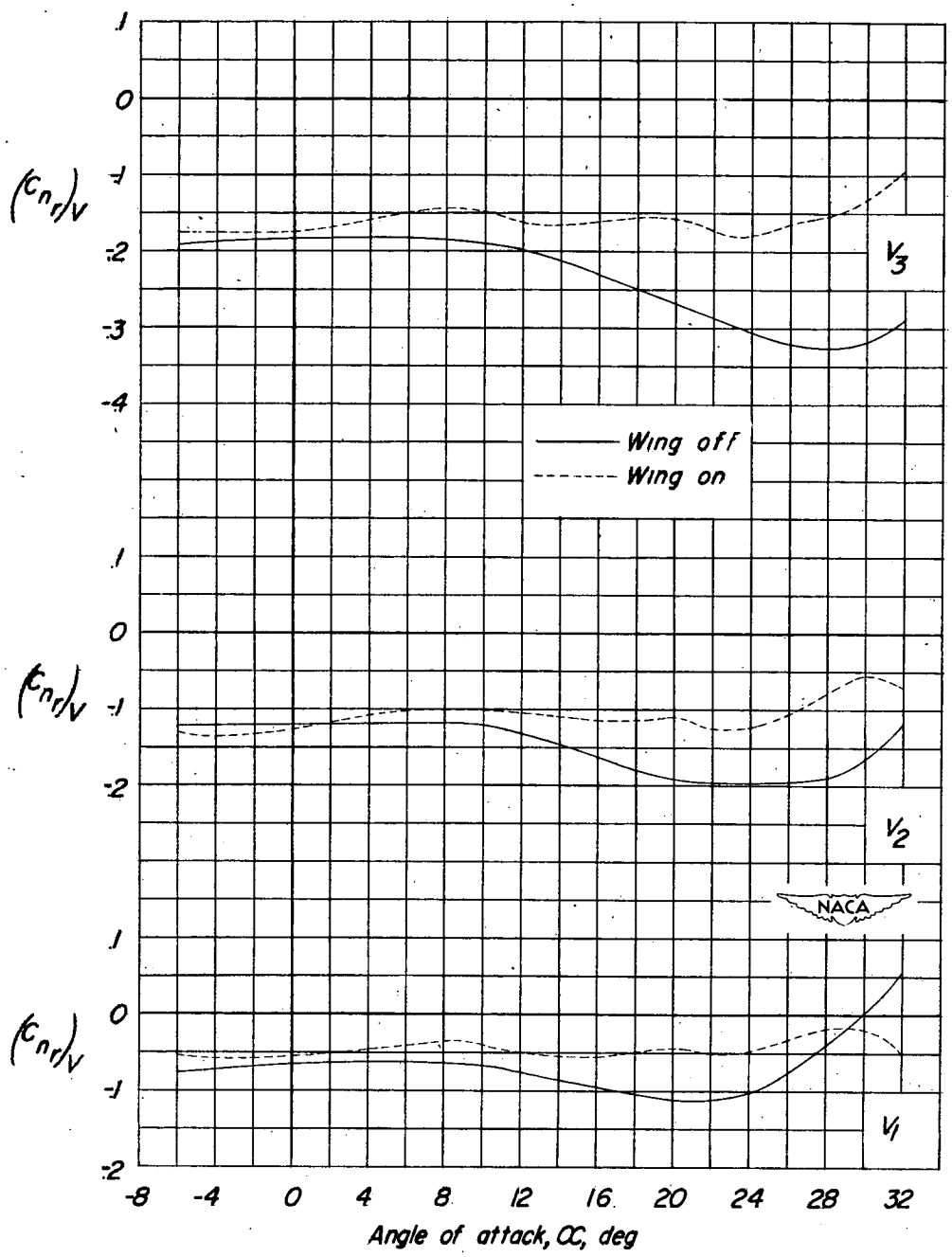

(b) Horizontal tail on.

Figure 19.- Concluded.

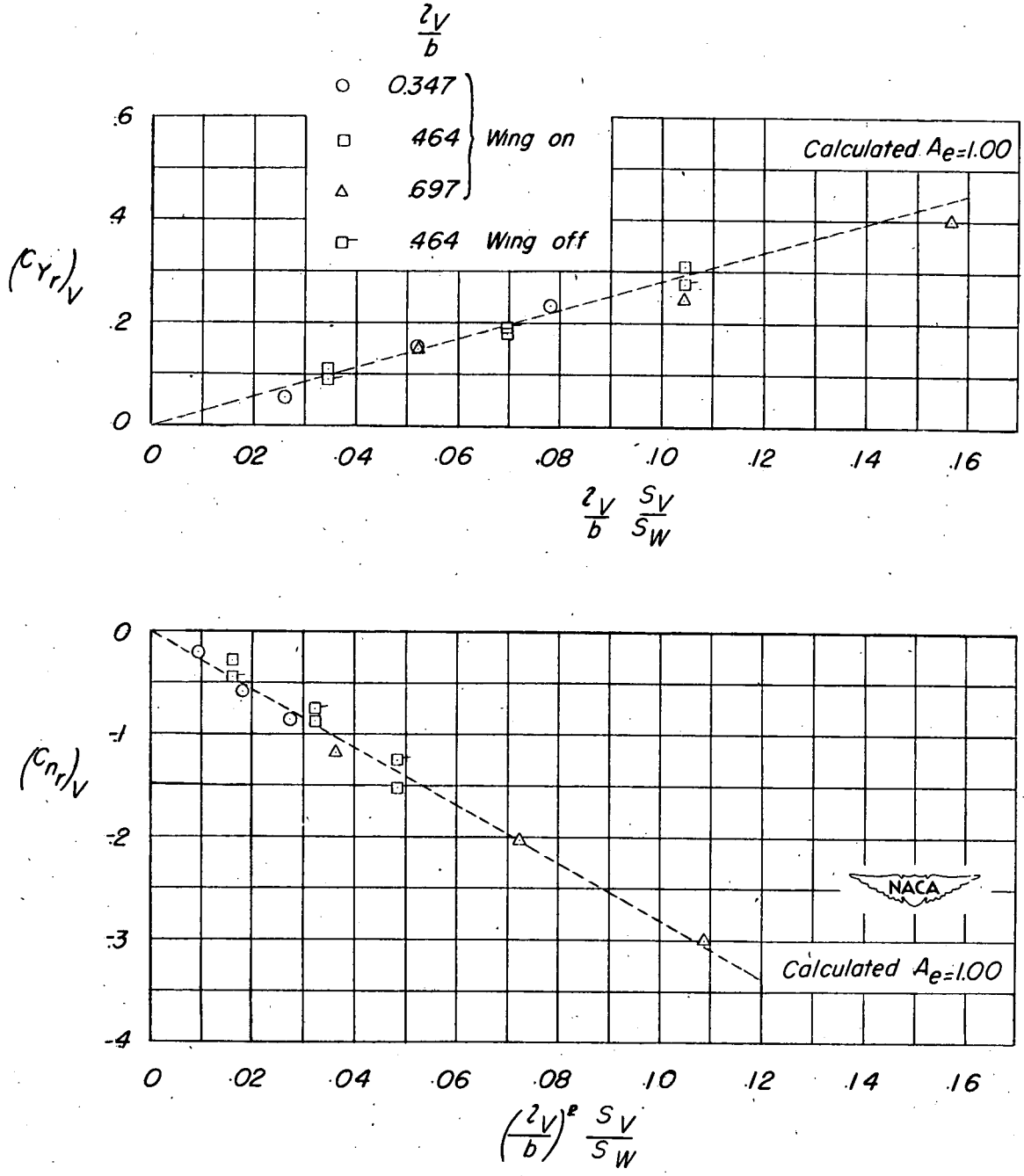

Figure 20.- Effect of tail area and tail length on $(C_{Y_r})_V$ and $(C_{n_r})_V$ at $\alpha = 0^\circ$. Horizontal tail off; wing slat off.

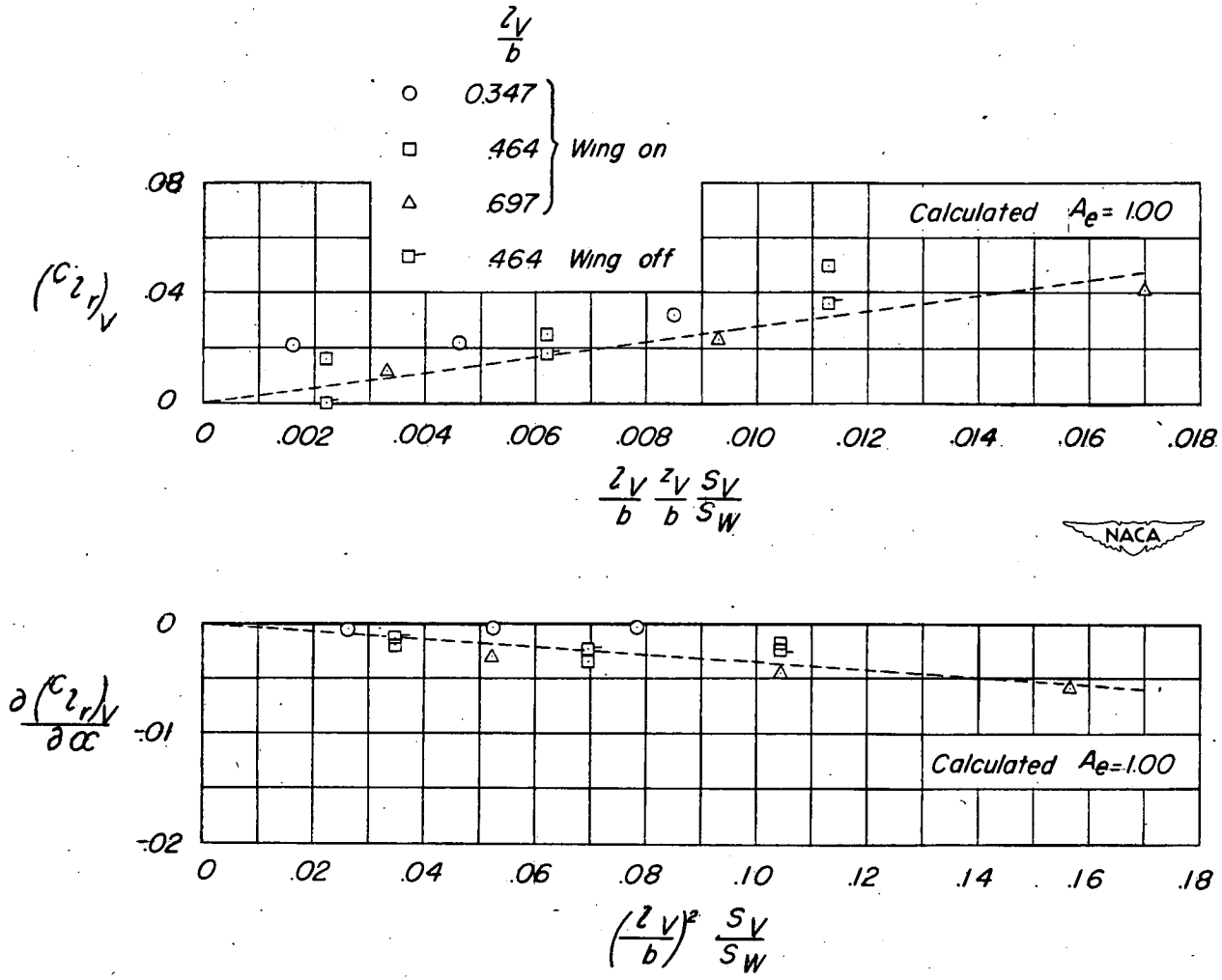

Figure 21.- Effect of tail area and tail length on $(C_{l_r})_V$ and $\partial(C_{l_r})_V/\partial\alpha$ at $\alpha = 0^\circ$. Horizontal tail off; wing slat off.

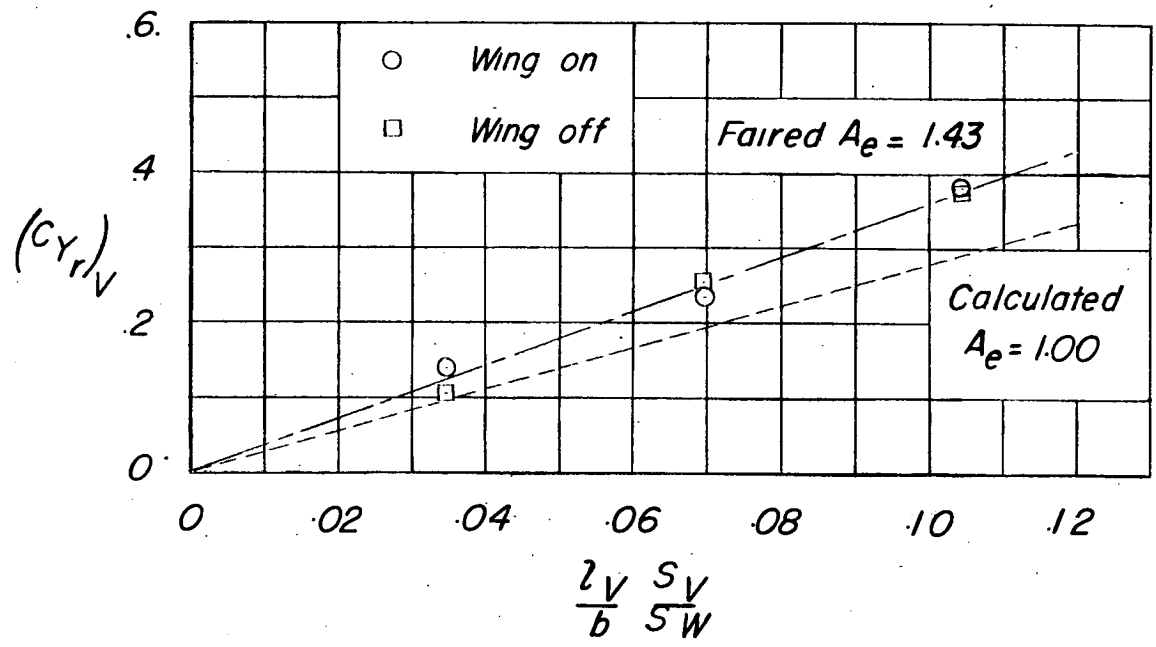

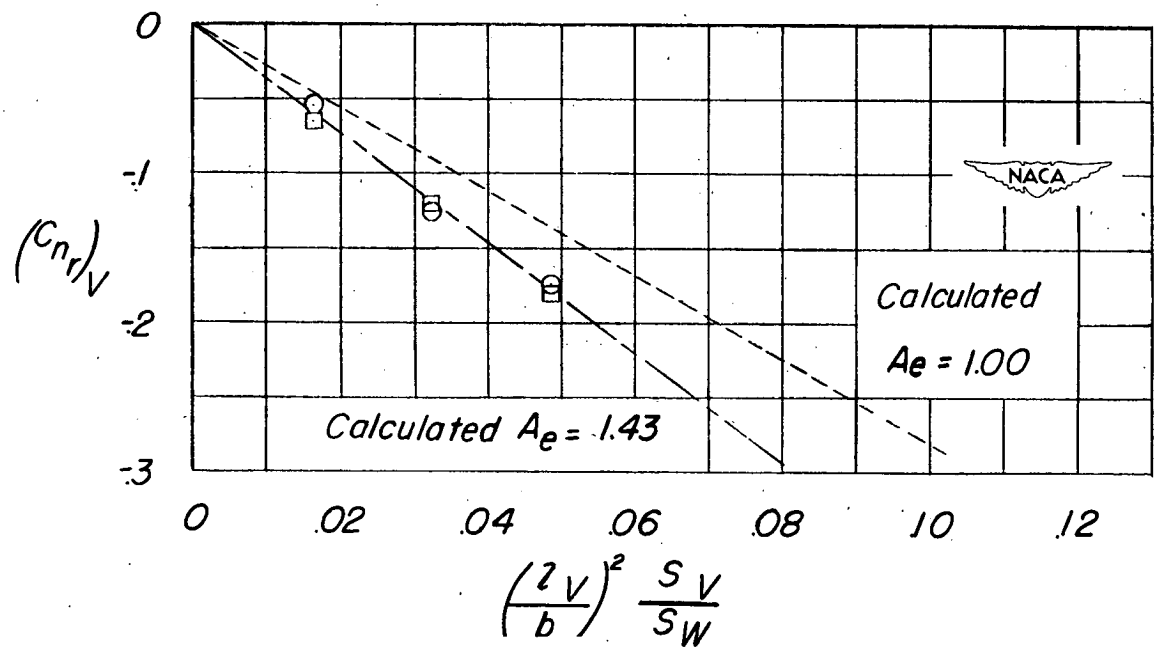

Figure 22.- Effect of tail area (wing on and off) on $(C_{Y_r})_V$ and $(C_{n_r})_V$ at $\alpha = 0^\circ$. Horizontal tail on; fuselage 2; $\frac{l_V}{b} = 0.464$; wing slat off.

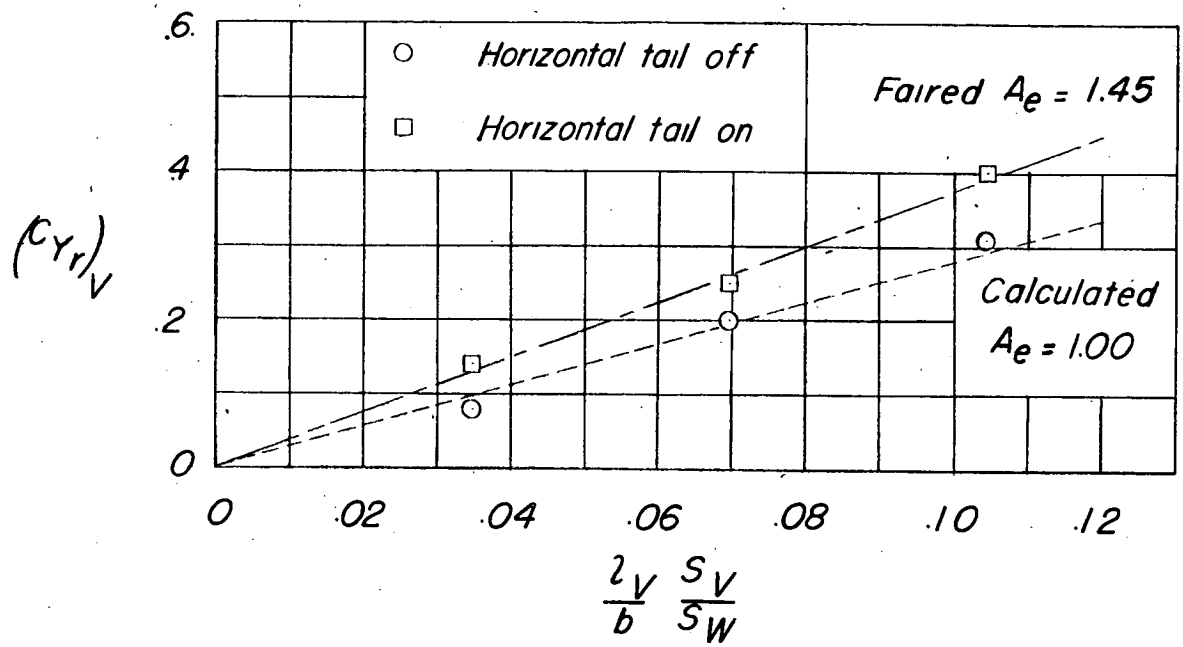

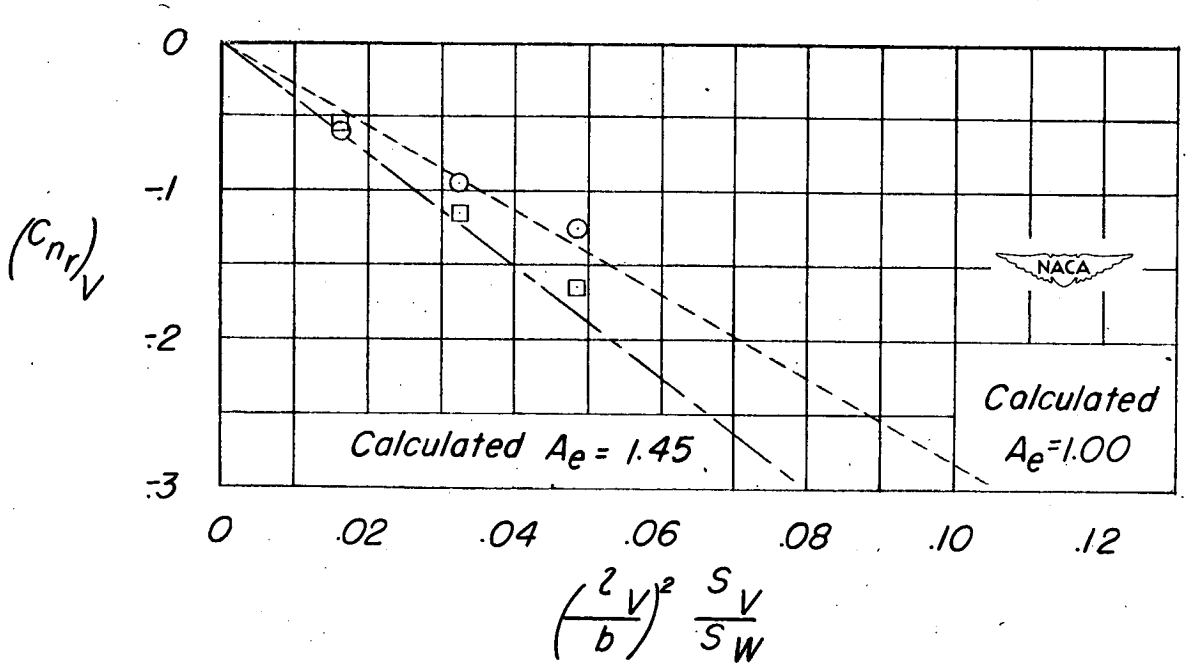

Figure 23.- Effect of horizontal tail on $(C_{Y_r})_V$ and $(C_{n_r})_V$ at $\alpha = 0^\circ$. Wing slat on; fuselage 2; $\frac{l_V}{b} = 0.464$.

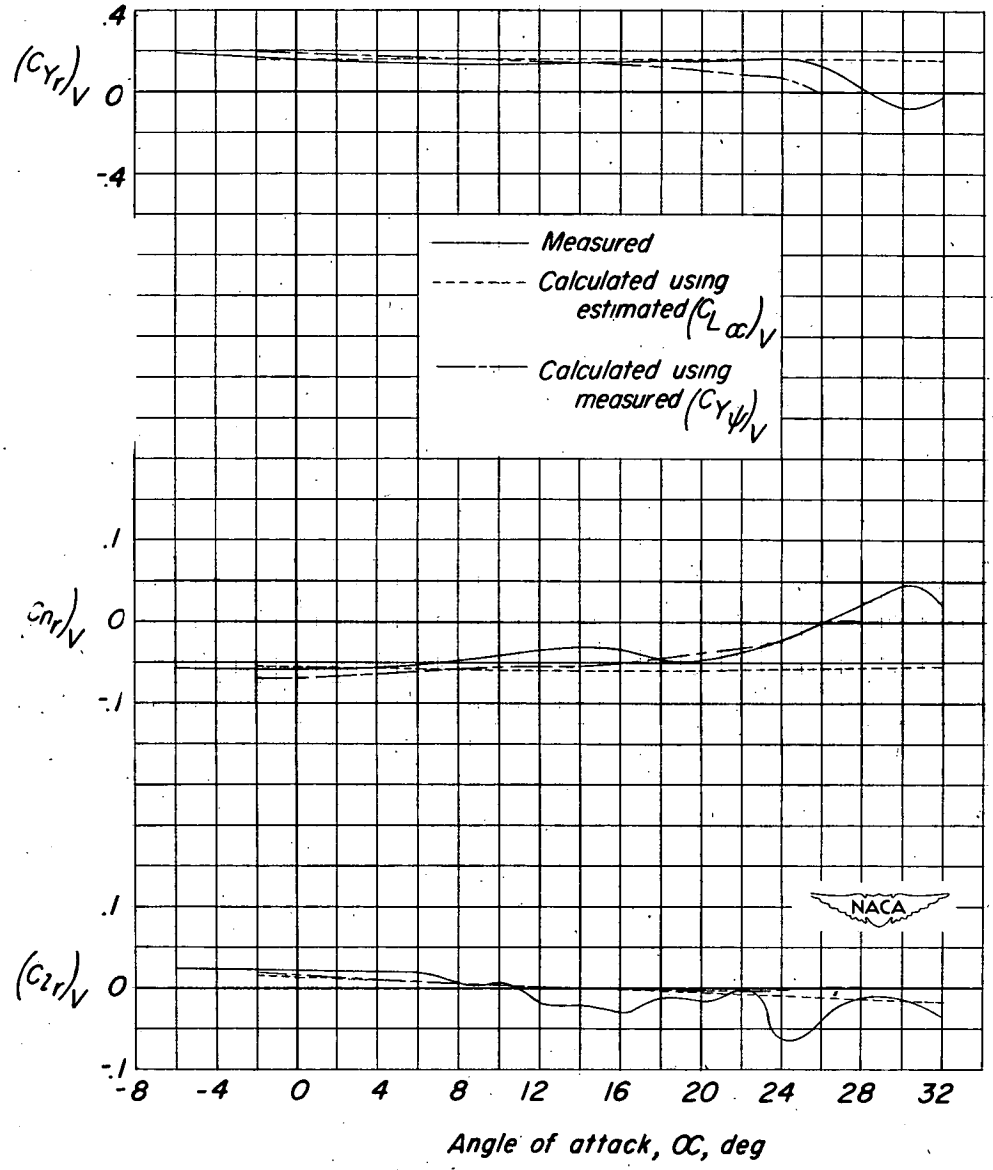

Figure 24.- Comparison of the measured and calculated variation with angle of attack of $(C_{Y_r})_V$, $(C_{n_r})_V$, and $(C_{l_r})_V$. Wing on, horizontal tail off; fuselage 1 $\left(\frac{i_V}{b} = 0.347\right)$; vertical tail 2 $\left(\frac{S_V}{S_W} = 0.150\right)$.

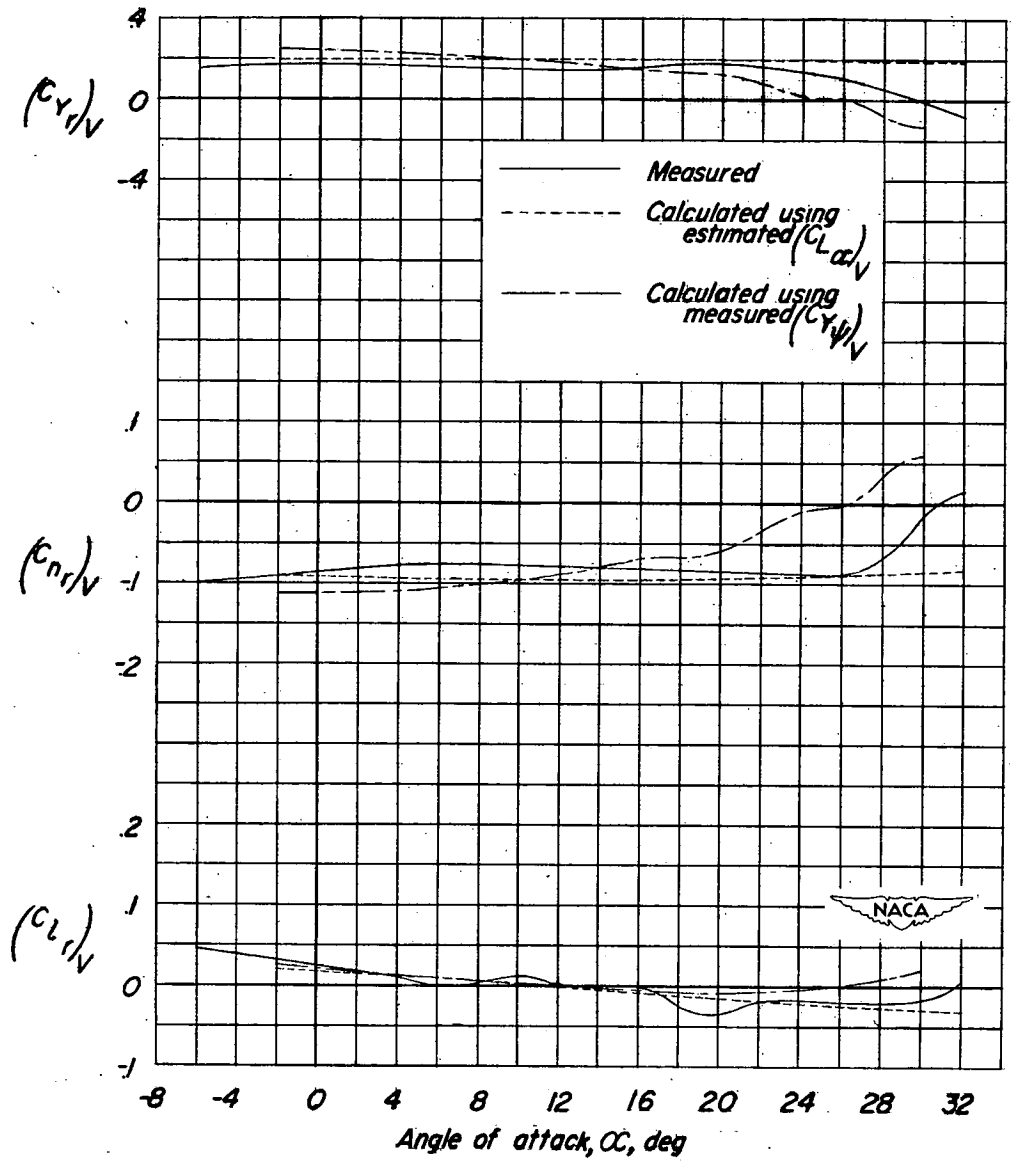

(a) Horizontal tail off.

Figure 25.- Comparison of the measured and calculated variation with angle of attack of $(C_{Y_r})_V$, $(C_{n_r})_V$, and $(C_{l_r})_V$. Wing on; fuselage 2 $\left(\frac{l_V}{b} = 0.464\right)$; vertical tail 2 $\left(\frac{S_V}{S_W} = 0.150\right)$.

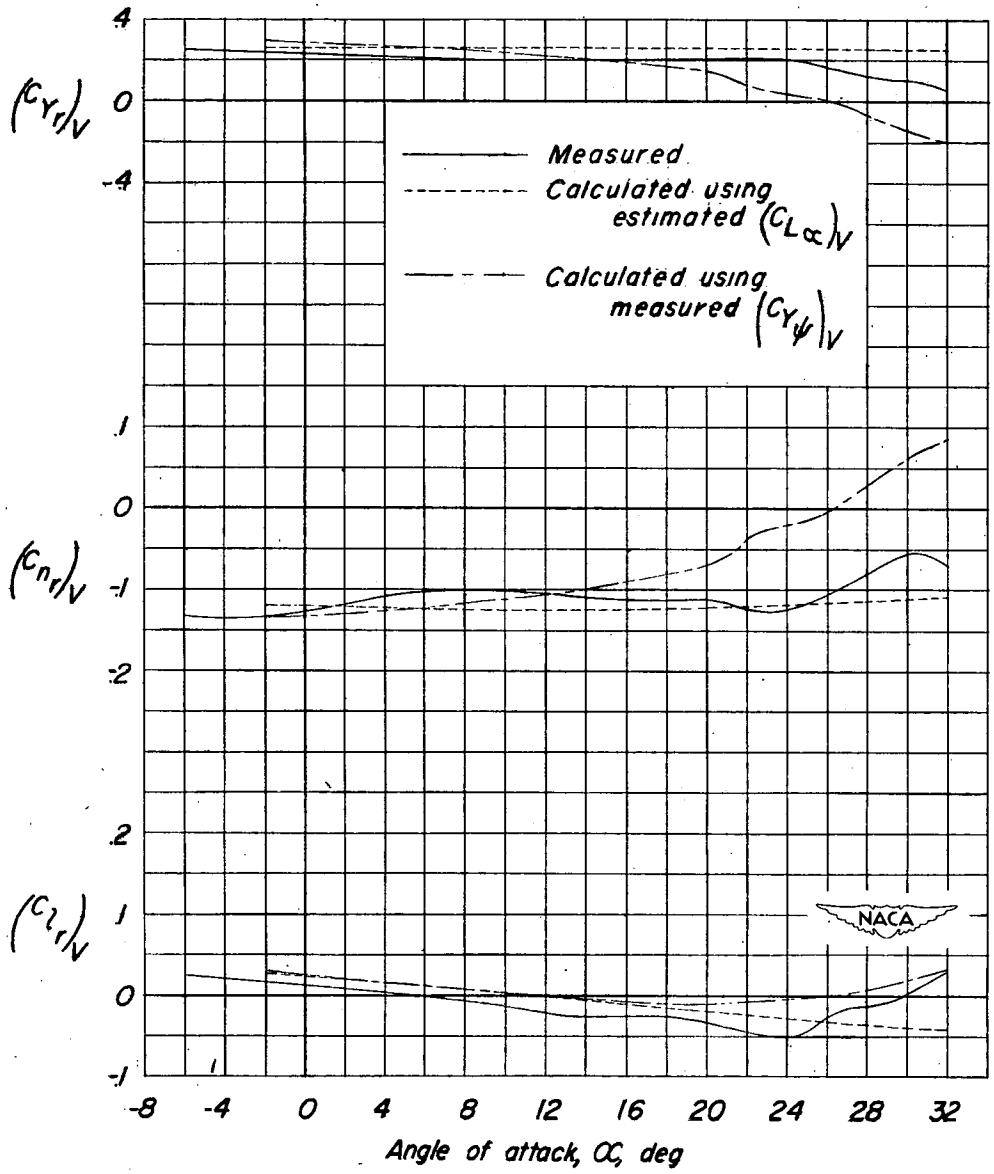

(b) Horizontal tail on.

Figure 25.- Concluded.

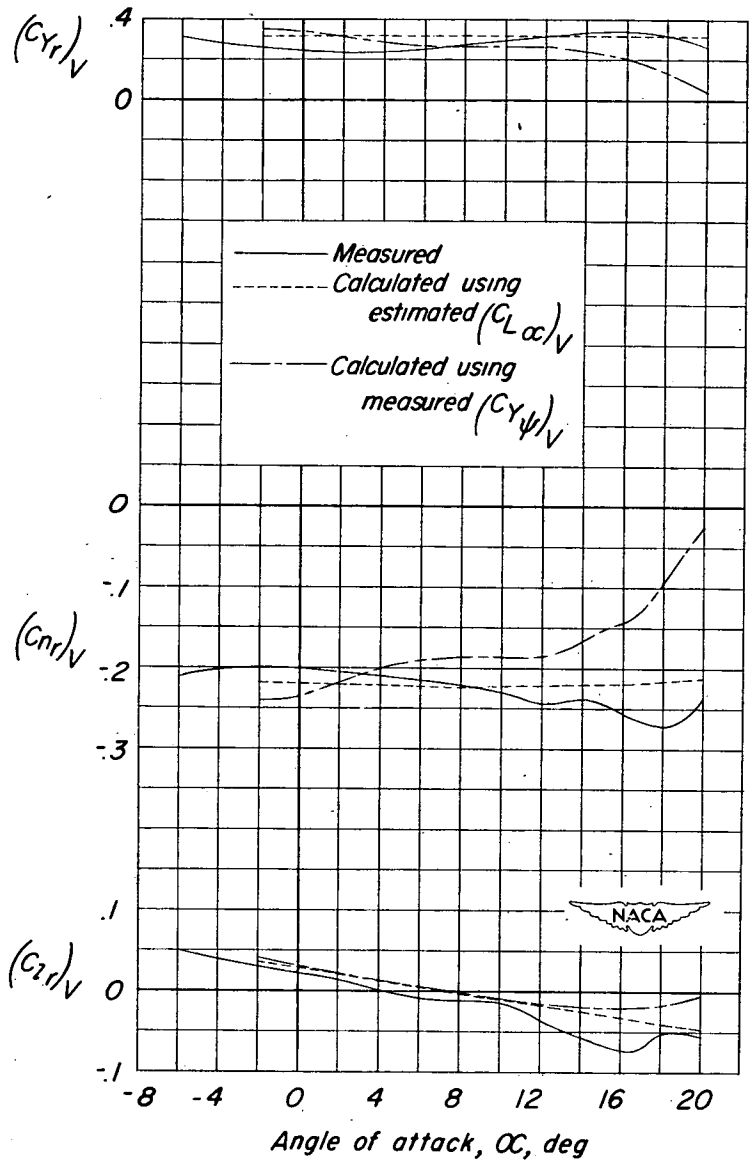

Figure 26.- Comparison of the measured and calculated variation with angle of attack of $(C_{Y_r})_V$, $(C_{n_r})_V$, and $(C_{l_r})_V$. Wing on; horizontal tail off; fuselage 3 $\left(\frac{l_V}{b} = 0.697\right)$; vertical tail 2 $\left(\frac{S_V}{S_W} = 0.150\right)$.

NACA-Langley - 5-14-51 - 1000